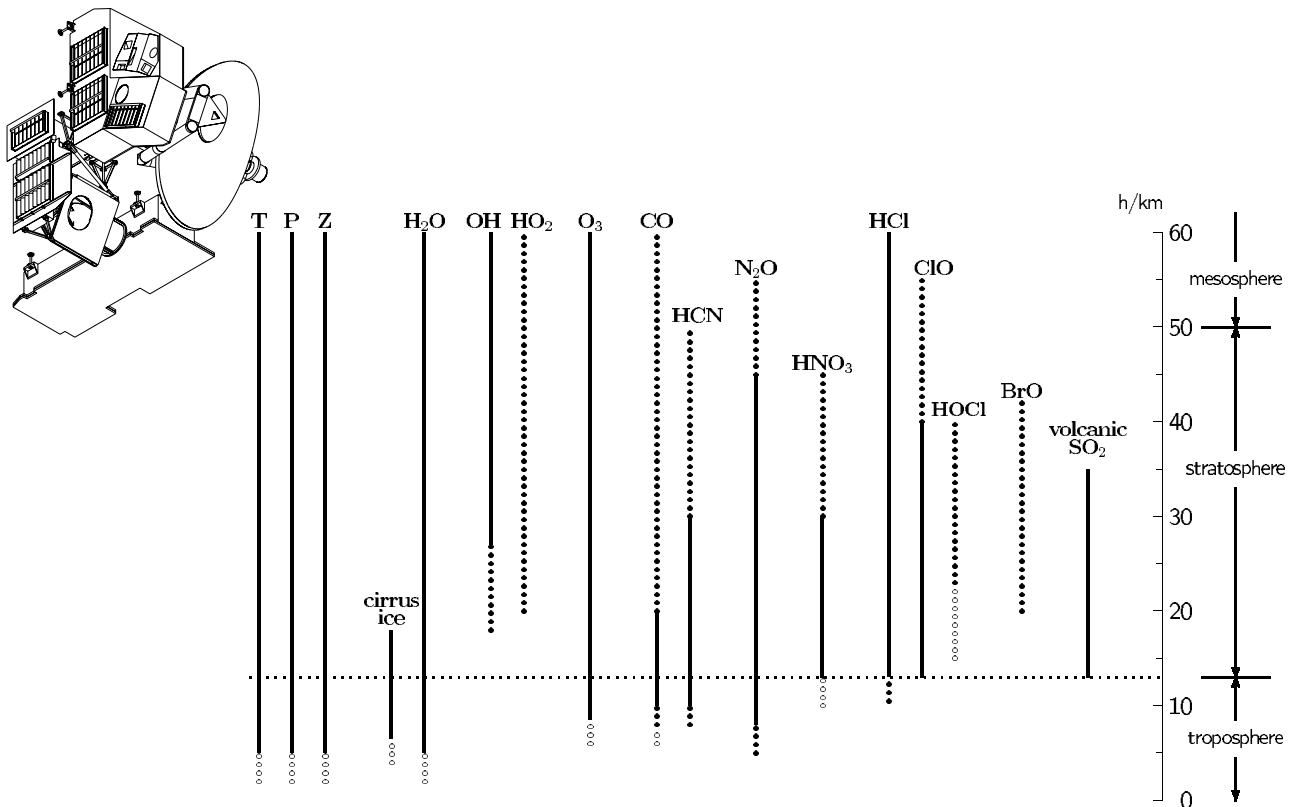**Earth Observing System (EOS)**

**Microwave Limb Sounder (MLS)**

# An Overview of the EOS MLS Experiment



Joe W. Waters

**Version 1.1**

15 October 1999

**JPL**

Jet Propulsion Laboratory
California Institute of Technology

Pasadena, California  91109-8099

**Release Record**

| Version | date released | comments |
|---------|---------------|----------|
| 1.0 | 15 Jan 1999 | Initial version |
| 1.1 | 15 Oct 1999 | Released following formal review of Version 1.0 by NASA board reviewing the EOS CHEM Algorithm Theoretical Basis Documents (ATBDs). This document received top grade of 'A' from the review board. The two recommendations by the board that apply to this document are italicized below, and are followed by the non-italicized response of the MLS team. |

| | | |
|---|---|---|
| | | • *A more complete (compared to that in the ATBD's) validation plan should be developed for the experiment.* This has been planned all along, and is being done. The EOS MLS data validation plan is a separate document. |
| | | • *It might be prudent to use a prototype 240 GHz radiometer to make balloon or aircraft measurements prior to launch to ensure there are no surprises in this region of the spectrum.* Although this would possibly be a worthwhile activity, it is outside the scope of available resources and time. The lines to be measured by the 240 GHz radiometer are strong, and the spectral region has been sufficiently characterized in the laboratory that we feel the risk of surprises is acceptably small, and any that occur can be adequately accommodated after launch (as was done for UARS MLS in the case of volcanic $SO_2$, $HNO_3$, upper tropospheric water vapor and $CH_3CN$). |

No changes to the document were needed as a result of these recommendations.

Changes from Version 1.0 are described below, and reflect expected progress since its release.

General changes:

(a) Titles for the categories of scientific objectives have been updated (in sections 1 and 4). Discussion of the objectives, in section 4, has been rewritten around key scientific questions.

(b) The 'secondary' geophysical data products of Version 1.0 have now been set as standard data products, and 'secondary' products have been deleted. This resulted in updates to (1) overall schedule in section 1, (2) text and table 5-1 in section 5.1, and (3) section 8.

(c) Updates made, as needed, for references and personnel. Formats of some tables changed. Relatively insignificant updates to some figures and tables.

Additional specific changes:

(1) Section 3: rearranged order of figures; added Figure 3-5 and text addressing stability of antenna reflectivity and its contribution to calibration stability.

(2) Added sentences in first paragraph of section 5.1 stating the reasons for choosing the particular radiometers.

(3) Table 5-5 giving estimated power, mass and data rate updated to the 'best estimates' presented at September 1999 MLS Critical Design Review, and current allocations have been added. These estimates are now well within the current allocations, but time-sharing is still identified to give 10% margin on power required at this stage of development.

(4) Added sentences at end of section 7.1 stating that production data processing will be done at the MLS Science Investigator-led Processing System (SIPS) in Pasadena, California, and that the data will be transferred to the GSFC DAAC for archive and public distribution.

# TABLE OF CONTENTS

# 1. Introduction

This document gives an overview of the Earth Observing System (EOS) Microwave Limb Sounder (MLS) experiment. The document is intended to provide information for a wide range of readers including MLS team members, additional scientists who may be using MLS data in their research, and programmatic officials. It also provides introductory and supporting information for the EOS MLS Data Processing Algorithm Theoretical Basis Documents by Filipiak (1999), Jarnot (1999), Jiang (1999), Livesey and Wu (1999), and Read et al. (1999).

EOS MLS is on the NASA EOS CHEMISTRY (CHEM) satellite mission currently scheduled for launch in December 2002, with an operational period extending at least 5 years after launch. The overall scientific objectives of the EOS MLS investigation are to provide crucial information for

- determining if stratospheric ozone is recovering as expected,
- improving knowledge of processes that affect climate variability, and
- helping understand ozone pollution in the upper troposphere.

These objectives are described further in sections 4.1 to 4.3.

EOS MLS and the CHEM mission contribute to the following three of the four areas of 'particular scientific and practical importance' identified in the US Global Change Research Program (Subcommittee on Global Change Research 1998):

- changes in ozone, UV radiation, and atmospheric chemistry,
- decade-to-century climate change,
- seasonal-to-interannual climate variability.

EOS MLS is a greatly enhanced version of the Upper Atmosphere Research Satellite (UARS) MLS experiment. It provides measurements of several stratospheric chemical species ($O_3$, $H_2O$, OH, $HO_2$, CO, HCN, $N_2O$, $HNO_3$, HCl, HOCl, ClO, BrO, volcanically-injected $SO_2$), temperature and geopotential height. It measures upper tropospheric $H_2O$, temperature, $O_3$, CO, HCN, $N_2O$, HCl (all of which can be made even in the presence of ice clouds), cirrus ice and geopotential height. Mesospheric temperature, $H_2O$, OH, $HO_2$, $O_3$, HCl, CO and geopotential height can also be measured to provide information on this higher region of Earth's atmosphere. The EOS MLS data will be made available publicly to the international scientific community.

The experiment is a collaboration between the United States and the United Kingdom. The California Institute of Technology Jet Propulsion Laboratory (JPL) has overall responsibility for its development and implementation. The University of Edinburgh (UE) Meteorology Department has responsibility for aspects of data processing algorithm development, data validation, and scientific studies.

Table 1-1 lists the formal investigator team for EOS MLS. It is anticipated, and encouraged, that many additional atmospheric scientists will become involved in using the MLS data as its operational phase approaches and its data become available.

Table 1-2 lists some EOS MLS Project key personnel.

Figure 1-1 gives the top-level schedule through 2 years after launch.

Table 1-1.  The Formal EOS MLS Investigator Team.

| name | organization | primary responsibility |
|---|---|---|
| J.W. Waters | JPL | US Principal Investigator |
| R.S. Harwood | UE | UK Principal Investigator |
| R.E. Cofield | JPL | Optics design, field-of-view calibration, geopotential height |
| M.J. Filipiak | UE | CO and upper trop $O_3$ products, algorithm development |
| L. Froidevaux | JPL | Stratospheric $O_3$, HCl, and HOCl products, data trends |
| R.F. Jarnot | JPL | Instrument Scientist, radiometric and spectral calibration |
| N.J. Livesey | JPL | Retrieval theory and algorithms, $N_2O$ and BrO products |
| H.M. Pickett | JPL | 2.5 THz system, OH and $HO_2$ products |
| H.C. Pumphrey | UE | Stratospheric $H_2O$ and HCN products, algorithm development |
| W.G. Read | JPL | 'Forward model', upper tropospheric $H_2O$ product |
| M.L. Santee | JPL | $HNO_3$ and ClO products, polar process studies |
| P.H. Siegel | JPL | Radiometer technology |
| D.L. Wu | JPL | Temperature, pressure, and cirrus ice products |

Table 1-2. Some Key EOS MLS Project Personnel.

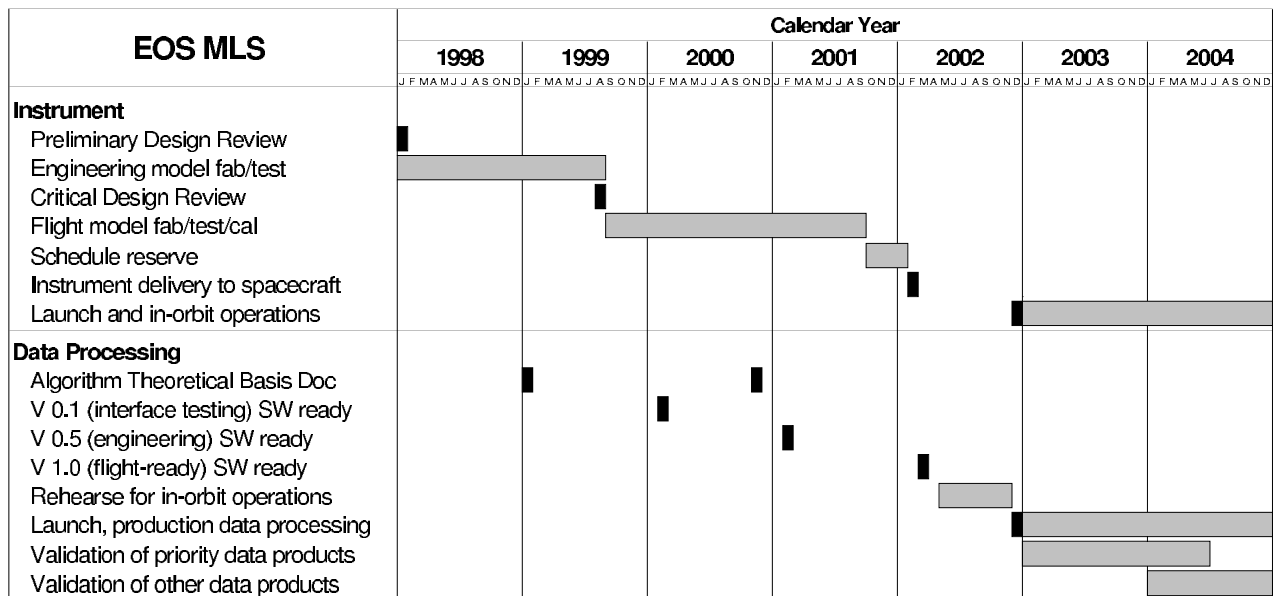| name | organization | position |
|---|---|---|
| G.K. Lau | JPL | EOS MLS Project Manager |
| D.A. Flower | JPL | EOS MLS Instrument Manager |
| M.A. Boyles | JPL | EOS MLS Instrument System Engineer |
| D.T. Cuddy | JPL | EOS MLS Science Software and Data Processing Manager |
| J.A. Kriz | JPL | JPL EOS MLS Science Computing Facility Manager |
| A. M. Brignall | UE | UE EOS MLS Science Computing Facility Manager |



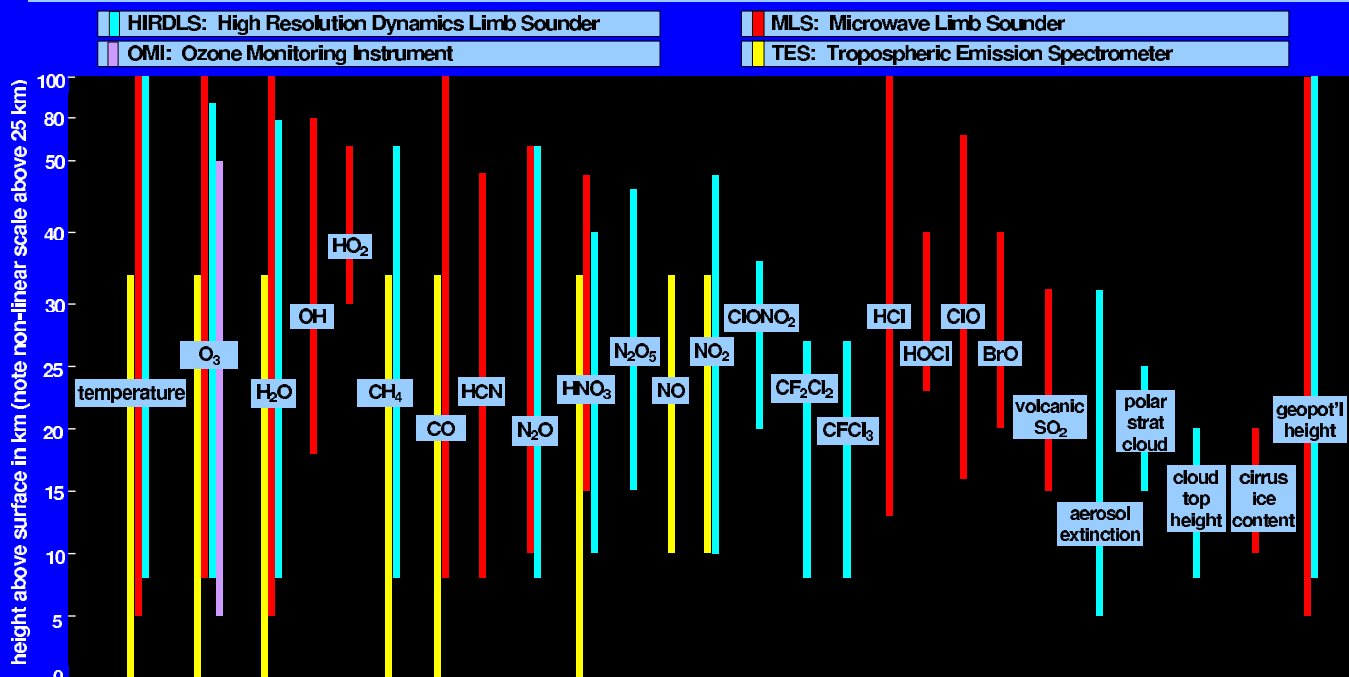Figure 1-1.  The EOS MLS top-level schedule through 2 years after launch.

Figure 1-2 (color). EOS CHEM atmospheric measurements. Note the non-linear vertical scale above 25 km.

Companion instruments to MLS on the CHEM satellite are the infrared High Resolution Dynamics Limb Sounder (HIRDLS), the infrared Tropospheric Emission Spectrometer (TES), and the ultraviolet Ozone Monitoring Instrument (OMI). HIRDLS provides unique high-resolution measurements that are important for improving understanding of the dynamics of the upper troposphere and stratosphere, and provides additional stratospheric species not measured by MLS. TES provides unique global measurements of tropospheric chemical species for improving understanding of tropospheric chemistry. OMI measures total column ozone, continuing the long record from the Total Ozone Mapping Spectrometer (TOMS), and also provides information on the vertical distribution of ozone; it has heritage from the TOMS instruments (e.g., McPeters et al. 1996), and from the Global Ozone Monitoring Experiment (GOME) instrument (Burrows et al. 1999) on the European ERS-2 satellite. The four CHEM instruments synergistically provide a powerful set of measurements for improving our understanding of atmospheric global change. Figure 1-2 shows the full suite of CHEM measurements. Sections 4 through 8 of this document describe the MLS measurements in detail.

The CHEM mission is managed by NASA's Goddard Space Flight Center. P. Sabelhaus is the CHEM Project Manager and M.R. Schoeberl is the CHEM Project Scientist. R.J. McNeal is the NASA Headquarters Program Scientist for CHEM. Information for the CHEM mission is available on the CHEM Project web site at http://eos-chem.gsfc.nasa.gov. M.D. King is the EOS Senior Project Scientist, and information for the overall EOS Project is on the web site maintained by his office at http://eospso.gsfc.nasa.gov. General information documents available there include the 350-page *1999 EOS Reference Handbook* and 400-page *EOS Science Plan*. Asrar and Dozier (1994) describe the overall EOS Science Strategy.

## 2. Heritage

EOS MLS has heritage from a number of aircraft and balloon experiments, and especially from the MLS experiment on the Upper Atmosphere Research Satellite (UARS).

Development of the MLS experiments began at the Jet Propulsion Laboratory in the mid-1970's and included instruments deployed on aircraft (e.g., Waters et al. 1979) and balloon (e.g., Waters et al. 1981) prior to application of the technique from space. The MLS instrument that was launched 12 September 1991 on UARS (e.g., Reber et al. 1993) is the first application of the microwave limb sounding technique from space. The instrument is described by Barath et al. (1993) and uses ambient-temperature double-sideband heterodyne radiometers that operate near 63 GHz, 183 GHz and 205 GHz. The primary data products for which UARS MLS was designed are stratospheric ClO, $O_3$, $H_2O$ and atmospheric pressure at the tangent point of the observation path (to provide a vertical reference for the other measurements). Temperature is also obtained from the 63 GHz radiometer that provides the pressure measurement.

Validation of the UARS MLS primary data products, and their accuracies and precisions, are described in the *Journal of Geophysical Research* special issue (volume 101, number D6, 30 April 1996) on UARS data evaluation: temperature/pressure by Fishbein et al. (1996); $O_3$ by Froidevaux et al. (1996) who also describe the retrieval algorithms that were used, Cunnold et al. (1996a,b), and Ricaud et al. (1996); $H_2O$ by Lahoz et al. (1996); ClO by Waters et al. (1996). Figure 2-1 shows the agreement obtained between MLS and some other well-calibrated measurements of the stratospheric $O_3$ profile. Additional data products obtained from UARS MLS, beyond those for which the instrument was primarily designed, include $SO_2$ injected into the stratosphere by volcanoes (Read et al. 1993), upper tropospheric $H_2O$ (Read et al. 1995), lower stratospheric $HNO_3$ (Santee et al. 1995), temperature variances associated with atmospheric gravity waves in the stratosphere and mesosphere (Wu and Waters 1996), detection of cirrus ice near the tropopause (D.L. Wu, manuscript in preparation), and tentative measurement of stratospheric $CH_3CN$ (N.J. Livesey, manuscript in preparation).

More than 130 refereed scientific publications using UARS MLS data have been published to date, and an updated publication list is kept on the MLS web site (http://mls.jpl.nasa.gov). Waters et al. (1999) give a summary of scientific results, and the following paragraphs discuss two examples.



Figure 2-1. Results of comparing UARS MLS Version 3 ozone with other well-calibrated near-coincident measurements (adapted from Froidevaux et al. 1996, and Cunnold et al. 1996a). Points A are the average differences for SAGE II measurements, selected in low-aerosol situations, covering 25 N to 55 N latitudes, and made between September 1991 and December 1993. Points T are average differences for 295 Table Mountain (34 N), California, lidar profiles. Points B are average differences for 42 Boulder (40 N) ozonesondes. Points U are average differences for 8 balloon-borne ultraviolet photometer profiles, and Points S are average differences for 5 balloon-borne submillimeter limb sounder profiles.
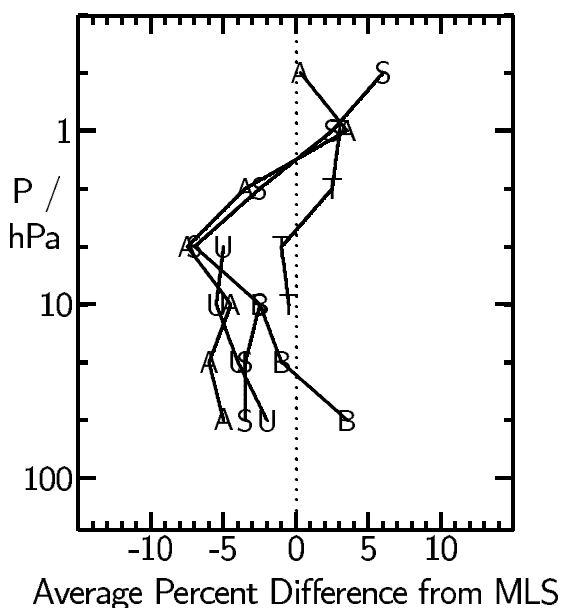
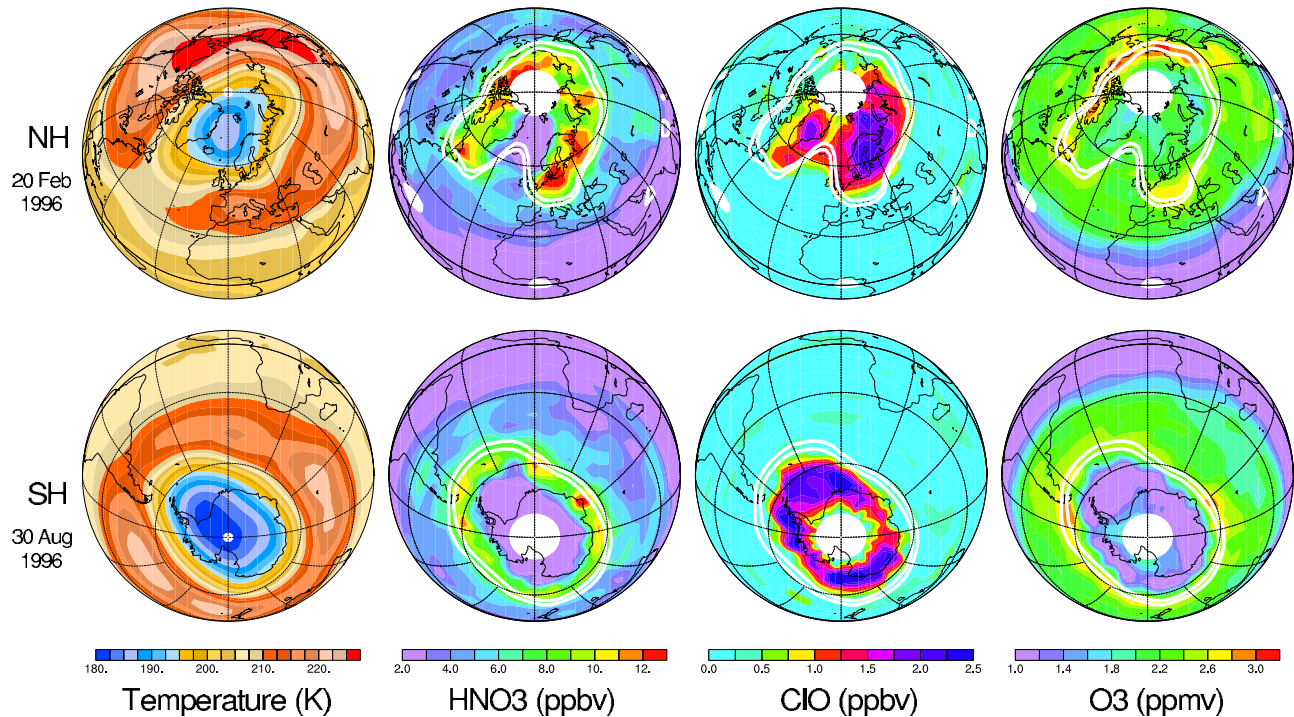# Earth's Lower Stratosphere in 1996 Northern and Southern Winters



Figure 2-2 (color). Earth's lower stratosphere in the Northern Hemisphere on 20 February 1996 (top) and in the Southern Hemisphere on 30 August 1996 (bottom). Measurements are interpolated to the 465 K potential temperature surface (~18 km), and white contours indicate potential vorticity values representative of the polar vortex edge. The $HNO_3$, ClO and $O_3$ data are from UARS MLS, and the temperature data are from operational analyses of the U.S. National Center for Environmental Prediction (NCEP). Temperatures in the blue and violet color ranges allow formation of polar stratospheric clouds from $HNO_3$ and $H_2O$; heterogeneous chemistry on these clouds leads to enhanced ClO that causes chemical depletion of $O_3$. $HNO_3$ also provides a source of $NO_x$, which quenches ClO and reduces the amount of ozone destruction. Both $HNO_3$ and $O_3$ increase in the lower stratospheric vortices during early winter due to downward transport of air rich in these species. The amount of ozone destruction each winter in the polar vortices depends on the duration of ClO enhancement, which is longer for the Antarctic than the Arctic. This difference is traceable to the Antarctic lower stratosphere being colder, and remaining cold for longer, than the Arctic. Occasional isolated large UARS MLS values of ClO outside the polar vortices are generally consistent with what could be caused by instrument noise (e.g., Schoeberl et al. 1993). M.L. Santee prepared this figure, taken from Waters et al. (1999).

Figure 2-2 illustrates some MLS results that have improved our understanding of global-scale destruction of ozone by chlorine chemistry. The MLS maps for 20 February 1996, one of the coldest days in the Arctic in recent years, show many similarities to the Antarctic in regards to processes leading to substantial ozone depletion, and substantial ozone loss in the Arctic has been detected (e.g., Manney et al. 1994). MLS measurements have shown that enhancement of ozone-destroying ClO throughout the Arctic winter vortex, as well as the Antarctic, is a recurrent feature. Only occasionally, however, have reductions in Arctic $HNO_3$ of the amount shown in the top row of Figure 2-2 been observed by MLS. The abundances of $HNO_3$ and ClO are very sensitive to temperature (for the range of temperatures experienced in the Arctic winter lower stratosphere), and even a small amount of cooling in the Arctic could cause much greater removal of Arctic $HNO_3$, longer duration of enhanced ClO and ozone destruction, and greater similarity to current conditions in the Antarctic.
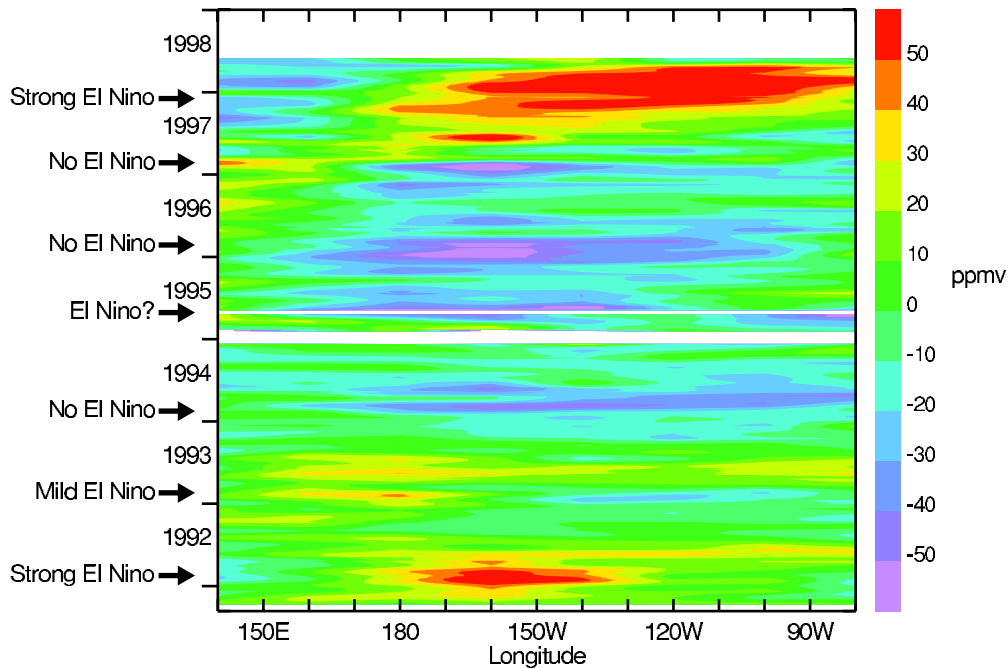
Figure 2-3 (color). Correlation between variations in tropical pacific upper tropospheric water vapor and El Niño sea surface temperature events. Data shown here are deviations from the mean in upper tropospheric water vapor at 215 hPa pressure (~11 km height) within 5 degrees of the equator as measured by UARS MLS. The vertical axis is time, covering late September 1991 through early June 1998. The horizontal axis is longitude in the tropical Pacific region. Labels along the left axis indicate whether or not an El Niño event in sea surface temperature occurred each year. Note the large increases in upper tropospheric water vapor during the 1991-92 and, especially, the 1997-98 El Niño events. W.G. Read prepared this figure, taken from Waters et al. (1999).

Figure 2-3 shows some UARS MLS results for upper tropospheric water vapor. Upper tropospheric water vapor, especially in the tropics, is thought to play a major role in feedback mechanisms affecting global warming. As is clear from this figure, there is strong correlation between El Niño sea surface temperature anomalies and upper tropospheric water vapor anomalies as observed by MLS. Improved understanding of these couplings, to which the MLS data are contributing, may help improve the ability to predict climate variations on seasonal-to-interannual time scales.

EOS MLS is improved over UARS MLS in having:

(1) additional stratospheric measurements for chemical composition and dynamical tracers,
(2) more and better upper tropospheric measurements,
(3) better global coverage and spatial resolution, and
(4) better precision for measurements of temperature, $O_3$, and ClO.

These improvements are possible because of:

(1) advances in microwave technology since development of the UARS instrument,
(2) better understanding of the technique's capabilities as a result of UARS experience,
(3) design of EOS MLS for upper tropospheric and lower stratospheric measurements,
(4) the EOS near-polar orbit which allows nearly pole-to-pole coverage on each orbit, and
(5) measurements being made in the orbit plane, allowing more accurate handling of gradients in the direction along the measurement track .

Measurements in the 640 GHz band to be used in EOS MLS have been made from balloon by Stachnik et al. (1992), and in the 2.5 THz OH band by Pickett (1999).
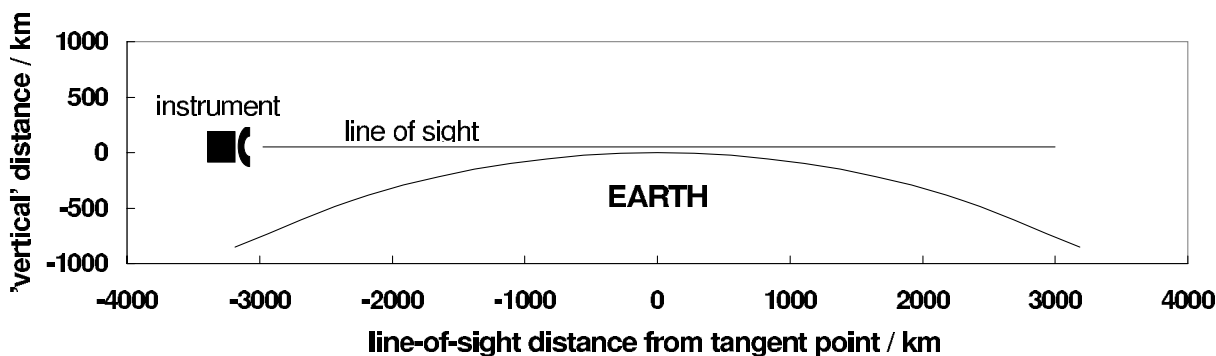
Figure 3-1. MLS measurement geometry. The geometry is drawn to scale with an instrument in 705 km altitude orbit (that of the EOS CHEM satellite) and the line of sight having 50 km tangent height. The size of the instrument is grossly exaggerated, of course. The orbit plane for EOS MLS is the plane of the paper, whereas for UARS MLS the orbit plane is perpendicular to the plane of the paper.

## 3. Measurement Technique

Microwave limb sounding obtains remote measurements of atmospheric parameters by observing millimeter- and submillimeter-wavelength thermal emission (radiances) as the instrument field-of-view (FOV) is scanned through the atmospheric limb from above. Figure 3-1 shows the geometry.

Features of the technique, described further by Waters (1993), include:

1. the ability to measure many atmospheric gases, with emission from molecular oxygen providing temperature and pressure;

2. reliable measurements, even in the presence of heavy aerosol, cirrus or polar stratospheric clouds that degrade shorter-wavelength ultraviolet, visible and infrared techniques;

3. the ability to make measurements at all times of day and night, and to provide global coverage on a daily basis;

4. the ability to spectrally resolve emission lines at all altitudes, which allows measurements of very weak lines in the presence of nearby strong ones and thus measurements of chemical species with very low atmospheric abundances;

5. composition measurements that are relatively insensitive to uncertainties in atmospheric temperature;

6. a very accurate spectral line data base (e.g., Pickett et al. 1992, Oh and Cohen 1994) [however better spectroscopic data are desired for tropospheric 'continuum' absorption];

7. instrumentation that has very accurate and stable calibration (For example, analyses of UARS MLS measured 'space radiances', as discussed later in this section, indicate less than 0.02% change in antenna mirror reflectivity over a 5-year period in orbit. This, in turn, implies an upper limit of 0.02% change in calibration due to mirror degradation, which is thought to be the largest contributor to calibration changes), and

8. instrumentation that has adequate sensitivity, without necessarily requiring cooling, and good vertical resolution set by size of the antenna.

The widths of spectral lines in the millimeter and submillimeter wavelength spectral regions used by MLS are dominated by pressure (collisional) broadening throughout the troposphere and stratosphere, resulting in the linewidth being a nearly exponential function of height up to~50-70 km. Doppler broadening dominates the linewidth at higher altitudes. Figure 3-2 on the next page shows linewidth variation with height for some representative spectral lines measured by EOS MLS.
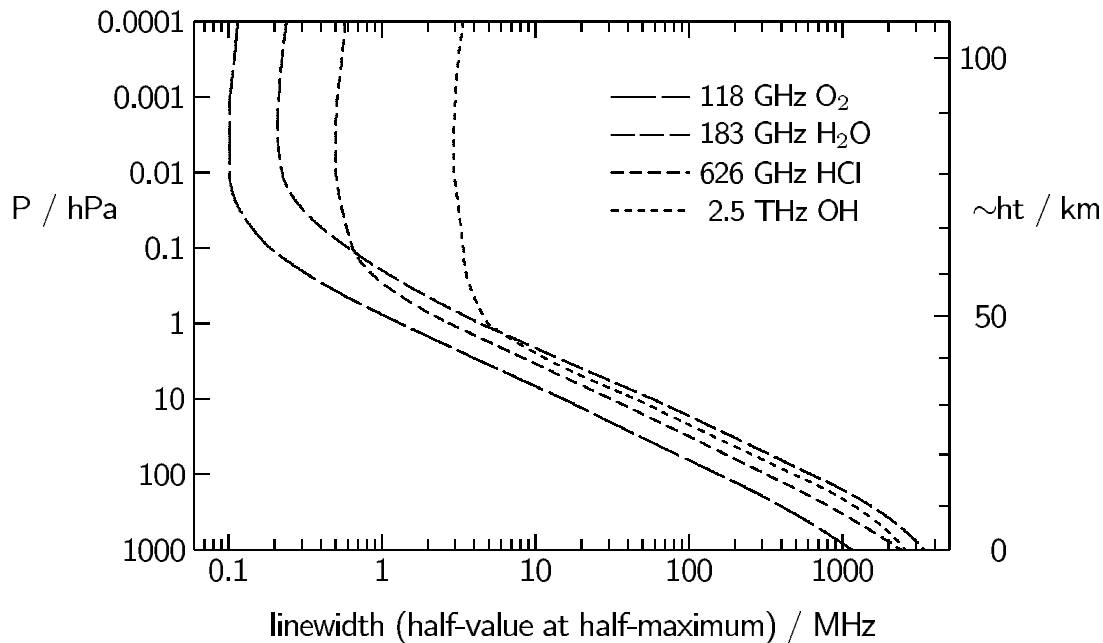
Figure 3-2. Spectral linewidth versus height for some spectral lines to be measured by EOS MLS.

Figure 3-3 below shows an example of spectra measured by UARS MLS, and illustrates the ability of the technique to spectrally resolve individual emission lines. Having several spectral channels covering a single emission line (and resolving this line at all altitudes of interest) provides robust measurements, since geophysical quantities can be obtained from the channel-to-channel spectrally-varying component of the measured thermal emission. Extraneous effects, such as stray radiation, generally have spectrally-flat emission over the spectral range used for measurements, and their uncertainties do not usually have first-order effects on the retrievals of geophysical parameters.

Figure 3-3. Stratospheric ozone emission line at 206 GHz measured by UARS MLS, and radiance residuals after retrieving the ozone profile. The vertical axis is (double-sideband) brightness temperature and the horizontal axis is frequency from line center. The thick horizontal bars indicate measurements from individual filters, all of which are measured simultaneously, and the horizontal width of each bar gives the spectral resolution of that filter. These measurements were made on 21 September 1991, shortly after initial in-orbit turn on of the UARS MLS instrument (and less than 10 days from launch). The 25-channel spectrometers used in EOS MLS will have 2.5 times the overall spectral bandwidth shown here to provide better measurements of broad spectral lines at lower altitudes.

Figure 3-4. MLS 205 GHz radiances (wing channel of ClO band) from the lower stratosphere (50 hPa tangent pressure) versus latitude for all measurements from all orbits on 21 September 1991. The tropical lower stratosphere had very heavy loading of aerosol from the Pinatubo volcano at this time. As anticipated on theoretical grounds, the MLS radiances are not noticeably affected by this aerosol layer, with an observational upper limit of ~0.1% opacity through the limb path. D.L. Wu prepared this figure, from Waters et al. (1999).

latitude region of very dense Pinatubo aerosol
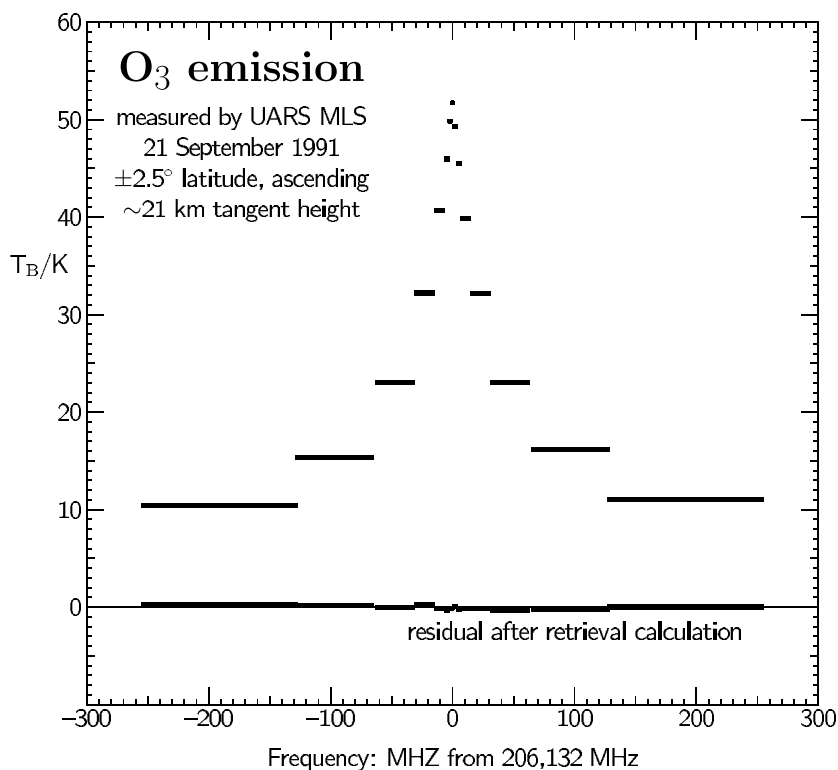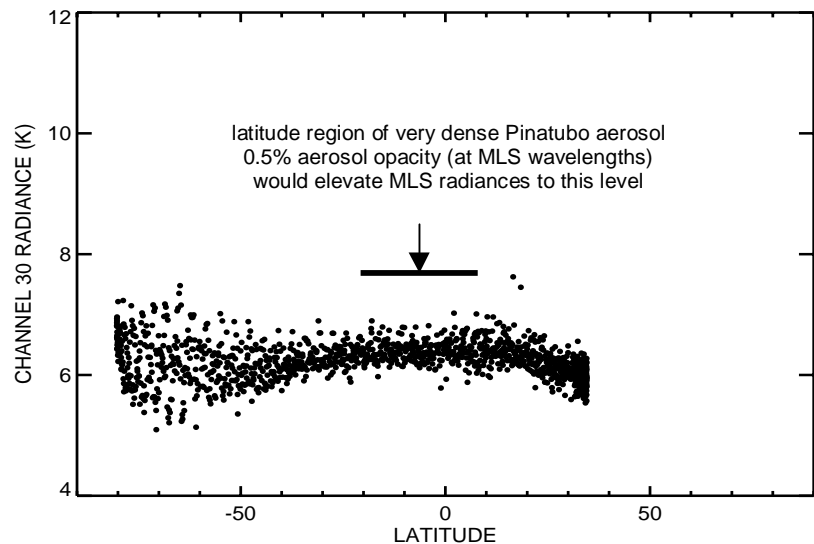0.5% aerosol opacity (at MLS wavelengths) would elevate MLS radiances to this level

Figure 3-4 above illustrates the insensitivity of measurements to volcanic aerosol by showing 205 GHz radiances from the lower stratosphere measured by UARS MLS when the tropics contained very heavy loading of aerosol from the Mt. Pinatubo volcano. No effect of the aerosol on the MLS radiances is seen, as expected from theoretical considerations, with an upper limit of ~0.1%. The ozone spectral line shown in Figure 3-3 was measured in the presence of this aerosol.

Figure 3-5 below shows data illustrating the excellent long-term stability of the UARS MLS antenna system reflectivity. 'Space radiances,' the radiances measured through the antenna system when it is pointed well above the atmosphere, are plotted. The typical in-orbit temperature of the antenna is ~250 K, and the slope of the best fit line, including its uncertainty, shown in Figure 3-5 thus corresponds to an upper limit of ~$3 \times 10^{-5}$ (= 0.007 K / 250 K) change per year in the overall antenna system reflectivity, or an upper limit of ~$2 \times 10^{-4}$ change over the ~5-year period analyzed. (Scatter in the points is due to limitations of the simple model used to remove cyclical, mainly 'UARS-monthly', temperature-dependent effects.) Degradation in reflectivity of the antenna reflector surfaces is thought to dominate any degradation in instrument radiometric calibration because these are the only surfaces in the signal path that are exposed to solar ultraviolet radiation and atomic oxygen. Changes in the antenna reflectivity affect overall radiometric calibration proportionally, and these data therefore imply an upper limit of ~$3 \times 10^{-5}$ per year (0.003% per year) degradation in UARS MLS radiometric calibration due to this effect. Similar performance is expected from EOS MLS.

Figure 3-5. Time-series of UARS MLS space radiances after applying a simple model to account for variation in temperature of the antenna. The marker on the left shows the effect that 0.1% change in reflectivity, with concomitant emissivity change, would have had. The nearly horizontal line is a best fit to the radiance trend over the ~5 year period analyzed; and has slope of -0.004 K/year with ±0.003 K/year 2σ uncertainty The data shown here are spectral averages for UARS MLS band 4 (206 GHz ozone spectral line). L. Froidevaux prepared this figure.

effect of 0.1% change in reflectivity
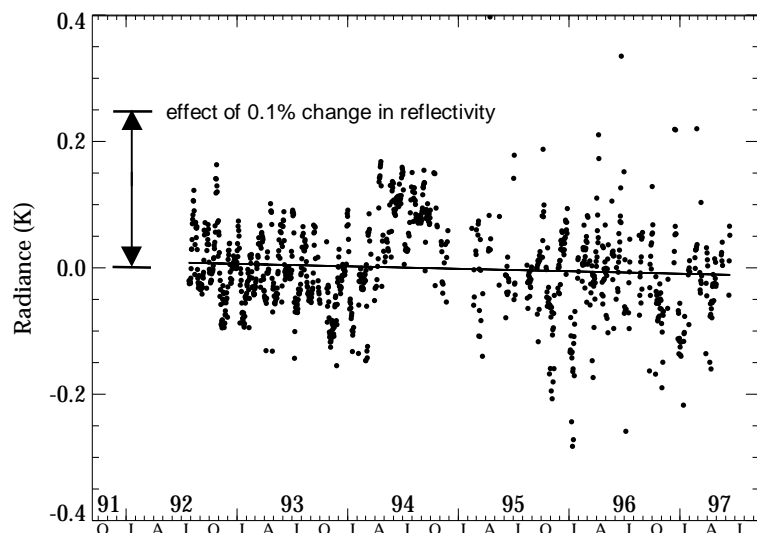
# 4. EOS MLS Scientific Objectives

As stated earlier in the introduction, the overall scientific objectives of the EOS MLS investigation are to provide crucial information for

- determining if stratospheric ozone is recovering as expected,
- improving knowledge of processes that affect climate variability, and
- helping understand ozone pollution in the upper troposphere.

The following subsections give more information on these objectives.

## 4.1 Determining if stratospheric ozone is recovering as expected

The stratospheric ozone shield is critical for protecting life on Earth. The abundance of ozone in the stratosphere is set by delicate balances between its production and destruction. It is now well-known, based on sound scientific evidence, that stratospheric ozone can be depleted by humankind's industrial activities. Solomon (1999) gives an excellent review of the concepts and history of ozone depletion.

International regulations have now limited the production of known ozone depleting substances. It is essential to determine if stratospheric ozone is recovering as expected. Some key questions include the following:

- Are stratospheric chlorine, ozone chemistry and ozone responding to regulations as expected?
- Will ozone recovery be delayed by climate changes? Climate changes which could delay the recovery include:
  (a) cooling of the lower stratosphere which could increase the formation of polar stratospheric clouds and the rate of heterogeneous reactions that destroy ozone,
  (b) increases of stratospheric $H_2O$ that could also increase the rate of formation of polar stratospheric clouds, and lead to greater abundance of stratospheric $HO_x$, both of which cause more ozone loss, and
  (c) changes in atmospheric circulation that could lead to a more isolated and colder Arctic vortex, and thus to more ozone loss in the northern hemisphere.
- Is the Arctic on the verge of severe denitrification, due to possible changes in climate, that could lead to increased ozone depletion?
- Do we adequately understand lower stratospheric chemistry at mid and low latitudes, and transport into these regions?
- Do we adequately understand upper stratospheric chemistry and transport?
- How will volcanic eruptions affect the recovery of stratospheric ozone?

EOS MLS stratospheric and mesospheric measurements that address these questions are:
$HCl$, $ClO$, $O_3$, $HNO_3$, $H_2O$, $N_2O$, $OH$, $HO_2$, $BrO$, $HOCl$, temperature, cirrus ice, geopotential height, volcanic $SO_2$.

EOS MLS will provide key measurements throughout the stratosphere to test our understanding of its chemistry, and provide new insights and early detection of (either expected or unanticipated) changes in chemistry of the stratosphere.

The lower stratospheric measurements are particularly important since they will occur during the time period when:

(1) lower stratospheric ozone, especially in the Arctic, is vulnerable to increased depletion due to effects of small decreases in temperature, due to possible changes in other parameters such as an increase in $H_2O$, and due to changes in circulation patterns (e.g., Shindell et. al. 1998);

(2) stratospheric chlorine loading is at or near its maximum; and

(3) some recovery of ozone at low altitudes in the Antarctic ozone hole might be detectable in the later portion of the mission (Hofmann 1996).

The simultaneous and commonly-calibrated MLS measurements of ClO, $HNO_3$, $H_2O$, HCl, $N_2O$, $O_3$ and temperature provide a powerful suite to improve understanding of key processes which could lead to greater ozone loss in the Arctic, and provide diagnostics of observed ozone loss. ClO abundances allow estimates of the amount of ozone loss due to chlorine chemistry (e.g., Mackenzie et al. 1996). Abundances of $HNO_3$ and $H_2O$, along with temperature, critically affect the microphysics leading to formation of cloud particle surfaces upon which heterogeneous chemistry can convert chlorine from reservoir to reactive forms. $HNO_3$ also provides a source of $NO_x$, which can affect the rate at which reactive chlorine is converted back to reservoir forms. Measurements of $N_2O$, a long-lived tracer, help separate chemical and dynamical causes of observed changes.

Measurements of OH, $HO_2$, BrO, and HOCl, along with those mentioned above, will improve our understanding lower stratospheric ozone changes at mid and low latitudes. The suite of measurements includes key species in the $HO_x$ and $ClO_x$ cycles now thought to dominate lower stratospheric ozone loss at mid to low latitudes. The ability of MLS to observe through dense aerosol is critical for monitoring stratospheric chemistry after any volcanic eruption that greatly increases stratospheric aerosol loading. EOS MLS data will provide a more stringent test of our understanding of upper stratospheric chemistry than has previously been possible.

The EOS MLS measurements of stratospheric OH will fill a serious gap in global observations to date because (as stated in the report from the *Workshop on Atmospheric Trace Gas Measurements for the Year 2000 and Beyond* published in the January/February 1995 issue of the EOS publication *The Earth Observer)*:

(1) OH controls the conversion of $CH_4$ to $H_2O$,

(2) reactions of $HO_x$ radicals are the most important loss mechanisms for ozone in both the lowest and highest regions of the stratosphere,

(3) reactions with OH control the rate of oxidation of sulfur gases ($SO_2$, OCS) to sulfate aerosol, and

(4) OH is in competition with heterogeneous chemistry in controlling the transfers between radical species in both the $NO_y$ and $Cl_x$ systems.

The report concludes that 'OH may be a well-behaved constituent under a wide range of circumstances, as must be assumed in models in absence of measurements to the contrary, but it is essential that this assumption be tested.'

The simultaneous measurements of $H_2O$, cirrus ice content, temperature, $O_3$, CO, HCN, $N_2O$ and HCl in the region of the tropopause should improve our understanding of exchange processes between the stratosphere and troposphere. The MLS measurements are especially important in the tropics since they can be made in the presence of cirrus which can degrade techniques based on measurements at ultraviolet, visible and infrared wavelengths.

Geopotential height measurements provide additional information on stratospheric dynamics.

## 4.2 Improving knowledge of processes affecting climate variability

Knowledge of upper tropospheric water vapor and its variations are crucial for understanding feedbacks associated with long-term climate change and couplings between the ocean and atmosphere which affect climate variability on seasonal-to-interannual scales. Upper tropospheric water vapor has been difficult to observe reliably on a global scale, but the capability of the MLS technique has been demonstrated by UARS MLS results. The MLS measurements are especially valuable because they can be made in the presence of cirrus where important processes affecting climate variability occur but where composition measurements from infrared, visible and ultraviolet techniques are limited by the presence of cirrus.

Some key questions in this area include the following:

- How do feedback mechanisms involving upper tropospheric $H_2O$ affect climate variability on a variety of time scales?
- What are the atmospheric processes that control upper tropospheric $H_2O$ abundances?
- How do variations in sea surface temperature affect upper tropospheric $H_2O$ (and thus climate)?
- How do lower stratospheric $H_2O$, and possibly $N_2O$ and Arctic vortex variations, affect climate?

EOS MLS upper tropospheric and lower stratospheric measurements to address these questions are:

$H_2O$, cirrus ice, temperature, $O_3$, and the tracers CO, HCN and possibly $N_2O$.
(Volcanic $SO_2$ may also be of value for improving our understanding of climate variability because it forms aerosol which in turn impact climate.)

The measurements of $H_2O$ in the upper troposphere are especially valuable because of uncertainties in climate feedback mechanisms associated with upper tropospheric $H_2O$ (e.g., Lindzen 1990), and because of the MLS ability to provide such measurements in the presence of cirrus and with good vertical resolution. Some of the more interesting phenomena related to climate variability and feedback are associated with the behavior of upper tropospheric water vapor in and around regions of deep convection in the tropics, where the presence of cirrus can degrade measurements by infrared, visible and ultraviolet techniques. Improved knowledge of upper tropospheric $H_2O$ in dry regions prevalent in the tropics and subtropics (e.g., Sandor et al., 1998) is also important for understanding climate variations. Pierrehumbert (1995) concludes that 'in the absence of these dry "radiator fins" maintained by subsidence, the tropical temperature would fall into a runaway greenhouse state that could be stabilized only by heat export to the extratropics.' He also identifies 'determination of the relative area of dry and subsiding versus moist and convecting regions of the tropics, and the degree of dryness of the subsiding regions' as 'key unsolved problems concerning the tropical climate.' EOS MLS data should solve these problems, at least in the upper troposphere.

The simultaneous MLS measurements of water in both the vapor and ice phases, along with temperature (and CO and HCN as tracers of air motion), should provide new information on processes affecting formation of cirrus ice particles that can have important climatic effects. They will be of value for improving our understanding of processes (such as El Niño) affecting climate variability on seasonal-to-interannual time scales.

$O_3$ and $N_2O$ in the lower stratosphere and upper troposphere may also affect climate and MLS measurements of these species will improve information on the distribution and variation of these species. Also, recent analyses has indicated that variations in the Arctic polar vortex may be instrumental in causing climate shifts associated with the 'Arctic oscillation' (Thompson and Wallace, 1998). MLS observations of various parameters (e.g., $N_2O$, geopotential height, temperature) will provide improved information on Arctic vortex dynamics.

The MLS temperature measurements complement those from infrared techniques in not being affected by variations in stratospheric aerosol content or $CO_2$, and complement those from nadir-looking microwave techniques in having better vertical (but poorer horizontal) resolution.

### 4.3  Helping understand ozone pollution in the upper troposphere

Ozone is a pollutant in the lower troposphere.  In the upper troposphere it is important because its photolysis by UV radiation in the presence of water vapor is the primary source of OH that is responsible for the oxidative removal of many polluting trace gases, and because it can influence climate (e.g., NASA, 1997).  Tropospheric ozone appears to be increasing, likely driven by anthropogenic emissions of $NO_x$, CO and hydrocarbons from fossil fuel combustion and biomass burning (e.g., Thompson 1992, Wang and Jacob 1998).  The increasing abundances of tropospheric $O_3$, $NO_x$, CO and hydrocarbons could affect the oxidizing (cleansing) capacity of Earth's atmosphere on a global scale, either decreasing or increasing it (Thompson, 1992).  Improving our understanding of tropospheric ozone chemistry and its global effects is essential for protecting the quality of the air we breathe.  Relatively rapid mixing in the troposphere implies that the upper troposphere, away from the immediate influence of localized sources, will be a good indicator of the global effects of regional pollution.  Some key questions in this area, which MLS data will help answer, include:

- What is the global distribution and variation of ozone in the upper troposphere?

- What are the dominant sources of upper tropospheric $O_3$?

- How is regional pollution related to global upper tropospheric $O_3$ pollution?

- How might increases in upper tropospheric $O_3$ affect global air quality?

EOS MLS upper tropospheric measurements that address these questions include:
$O_3$, CO, HCN - and possibly $H_2O$ and $N_2O$ as tracers to identify
air of stratospheric origin.

The simultaneous measurement of $O_3$, and of CO and HCN which serve as tracers of air mass tropospheric origin and motion, should provide new information on the global distribution, variation and sources of $O_3$ in the upper troposphere.  Some of the larger variations expected in upper tropospheric $O_3$ and CO due to biomass burning (e.g., Thompson et al. 1996; Pickering et al. 1996) should be detectable in daily maps from EOS MLS, but smaller variations will require maps built up from averages of observations over a longer period of time.  Geopotential height measurements provide additional information on upper tropospheric dynamics.

Cirrus clouds near the tropopause can potentially lead to the activation of chlorine and ozone loss at mid and low latitudes (Borrman et al. 1996), but models of this process (Solomon et al. 1997) fall short of explaining the pronounced minima in upper tropospheric $O_3$ detected in the presence of ice clouds by ground-based lidar at mid latitudes (Reichardt et al. 1996).  EOS MLS should help us to understand such phenomena on a global scale.  It concurrently measures $O_3$ and cirrus ice, as well as CO which can help identify regions of convective uplift where low $O_3$ might be due to dynamics.  CO and HCN can also identify air that has been influenced significantly by biomass burning.  EOS MLS also measures $N_2O$ and HCl which can help identify air of stratospheric origin and provide estimates of the amount of inorganic chlorine available for activation by heterogeneous chemistry.

The improved EOS MLS ability to measure stratospheric ozone column, over that of UARS MLS, should lead to better determinations of tropospheric ozone obtained from residuals between total column ozone measured by other sensors and the stratospheric column from EOS MLS.

## 4.4  Summary of EOS MLS measurement objectives

Figure 4-1 summarizes the EOS MLS scientific measurement objectives.  Accuracy and precision for the measurements are summarized in section 8.  Full details on precision for all measurements are given in Filipiak (1999).
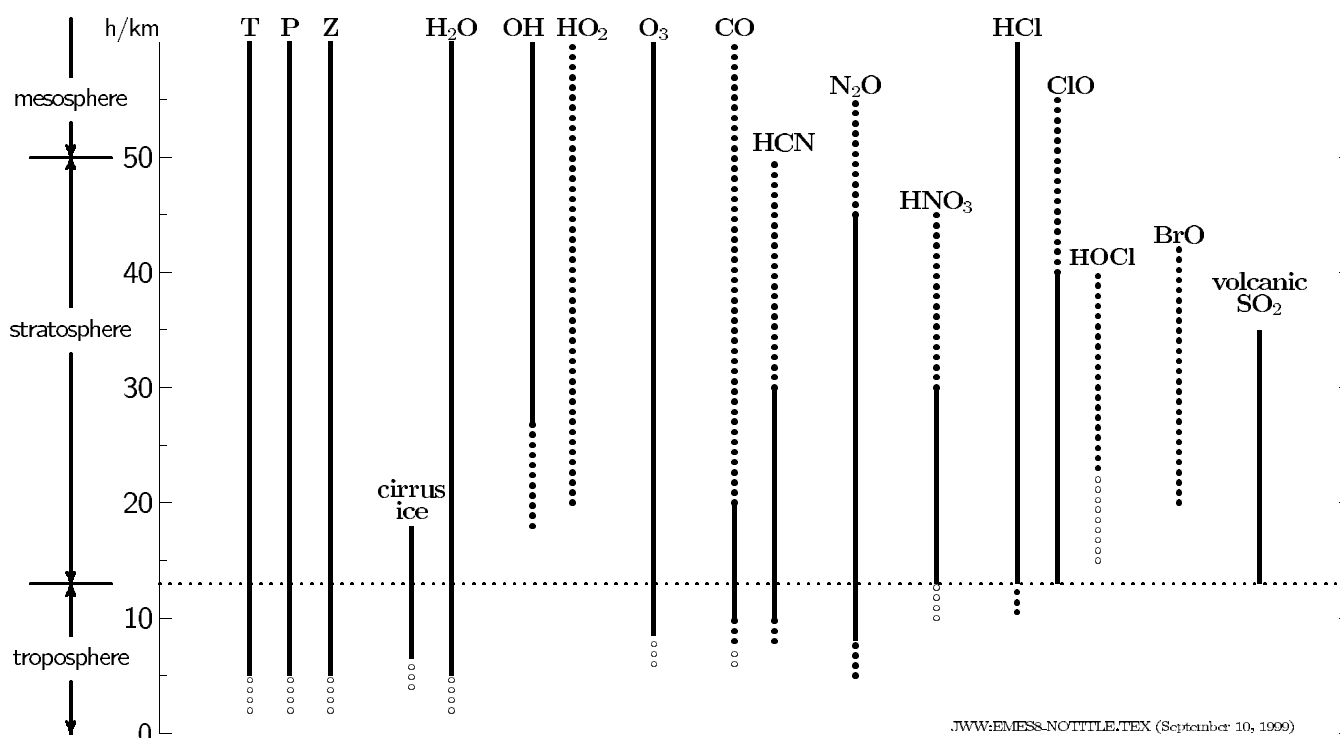


Figure 4-1.  EOS MLS scientific measurement objectives.  T is temperature, P is pressure, and Z is geopotential height.  Solid lines indicate useful individual profiles and/or daily maps. Dotted lines indicate that zonal (or other) averages will likely be needed to obtain useful precision.  Open circles indicate goals for more difficult measurements.  Measurements of T, P, Z, $H_2O$, $O_3$, HCl, OH and CO extend higher than the 60 km indicated here.  It should be noted that 'useful profiles' indicated by the solid lines here do not necessarily apply at all times of day and night due to diurnal variation in some species, particularly OH, $HO_2$, ClO and BrO.  Also, they do not necessarily apply at all latitudes due to latitudinal variation in abundances.  For example, although useful individual profiles of lower stratospheric $HNO_3$ will be obtained at mid and high latitudes, they are not expected in the tropics because of the smaller $HNO_3$ abundances at low latitudes.

# 5. The EOS MLS Instrument

## 5.1 Complement of radiometers

The EOS MLS instrument has radiometers in five spectral regions, chosen to produce the set of standard geophysical data products from MLS stated in Appendix D of the May 1995 EOS Execution Phase Project Plan (NASA Goddard Space Flight Center, 1995) and given below in Table 5-1. The 118 GHz radiometer, covering the strong 118 GHz $O_2$ line, is chosen to optimize trade-offs between precision and vertical resolution for temperature, geopotential height and tangent pressure. The 190 GHz radiometer is chosen to measure the 183 GHz $H_2O$ line, as done by UARS MLS, and to measure a strong band of $HNO_3$ lines. The 240 GHz radiometer is chosen to cover very strong $O_3$ lines in a spectral region where upper tropospheric absorption (mainly by water vapor continuum) is sufficiently small to allow measurements of upper tropospheric $O_3$. The 640 GHz radiometer is chosen to measure the lowest-frequency line of HCl, the strongest rotational line of ClO (more than 10× stronger than the 204 GHz line measured by UARS MLS), and a strong line of $N_2O$. The 2.5 THz is chosen for OH because of the relatively clean spectral region around the pair of very strong OH lines at 2.510 and 2.514 THz, and because of the availability of a $CH_3OH$ gas laser to use as local oscillator for this radiometer.

These radiometers provide additional measurements, indicated in the table, which are now standard data products for MLS as stated in the EOS Chemistry Project Plan (NASA Goddard Space Flight Center, 1999). Additional contributions from the radiometers are also stated in the table.

Advanced planar-technology mixers (Siegel et al. 1993) are used in all the radiometers, with a monolithic millimeter-wavelength integrated-circuit (MMIC) amplifier (Weinreb et al. 1997) preceding the mixer in the 118 GHz radiometer. Subharmonically-pumped mixers are used at 118, 190, 240 and 640 GHz, and a fundamental mixer at 2.5 THz. Local oscillators are solid state, except at 2.5 THz which uses a $CO_2$-pumped methanol ($CH_3OH$) gas laser. All radiometers operate at ambient temperature.

Table 5-1. MLS geophysical data products and radiometers.

| MLS Standard Data Products from May 1995 EOS Project Plan, GSFC 170-01-01, Rev A | Radiometers required for Standard Data Products in left column | Additional measurements by the radiometers, set as Standard Data Products for MLS in the April 1999 CHEM Project Plan | Additional contributions by the radiometers |
|---|---|---|---|
| temperature, geopotential height | 118 GHz | contributes to cirrus ice product | provides tangent pressure measurement needed for all other measurements, improves quality of upper trop $H_2O$ |
| $H_2O$ $HNO_3$ | 190 GHz | HCN, contributes to cirrus ice product | ClO (lower quality than from 640 GHz), $N_2O$ (lower quality than from 640 GHz), $O_3$ (but not in upper trop), $SO_2$ |
| $O_3$ | 240 GHz | CO, contributes to cirrus ice product | temperature/pressure (over limited range with poorer quality than from 118 GHz), improves quality of upper trop $H_2O$ |
| HCl, ClO, $N_2O$ | 640 GHz | BrO, HOCl, $HO_2$, volcanic $SO_2$, contributes to cirrus ice product | stratospheric $O_3$ with better vertical resolution than 240 GHz (but does not measure $O_3$ in upper troposphere), improves quality of upper trop $H_2O$ |
| OH | 2.5 THz | | pressure over limited vertical range (needed from 2.5 THz radiometer for OH measurement) |

## 5.2 Signal flow

Figure 5-1 shows a signal flow block diagram for the instrument. Atmospheric signals for the 118, 190, 240 and 640 GHz radiometers are collected by a three-reflector antenna system which vertically scans the limb. The antenna design is very similar to that of UARS MLS, with a primary reflector dimension of 1.6 meter projected in the vertical direction at the limb tangent point. A switching mirror following the GHz antenna system provides radiometric calibration by switching to views of calibration targets or to space. An optical multiplexer, consisting of an arrangement of dichroic plates and polarization grids as shown in Figure 5-2, spatially separates the signal from the switching mirror into different paths feeding different radiometers. There is a second 118 GHz radiometer (at the orthogonal polarization) to provide redundancy for temperature and pressure which are needed for all the other measurements.

The atmospheric and calibration signals for the 2.5 THz radiometer are obtained via a dedicated telescope and scanning mirror whose operation is synchronized with that of the GHz antenna and the GHz switching mirror. The 2.5 THz primary mirror dimension in the 'limb vertical' direction is ~25 cm, and the field-of-view width at the tangent point is ~2.5 km. The 2.5 THz measurements are performed simultaneously at both polarizations to provide increased signal to noise for the important OH measurement.

The radiometers have intermediate frequency (IF) outputs in several bands as described later in section 5.3. These IF outputs are fed, via a switch network, to spectrometers. The switch network provides some redundancy, and can be used to improve efficiency if time-sharing of measurements is required because of power limitations (see section 5.8). Digitized data from the spectrometers are passed to the command and data handling system for transmission to the ground. The instrument individual measurement integration time is 1/6 second.
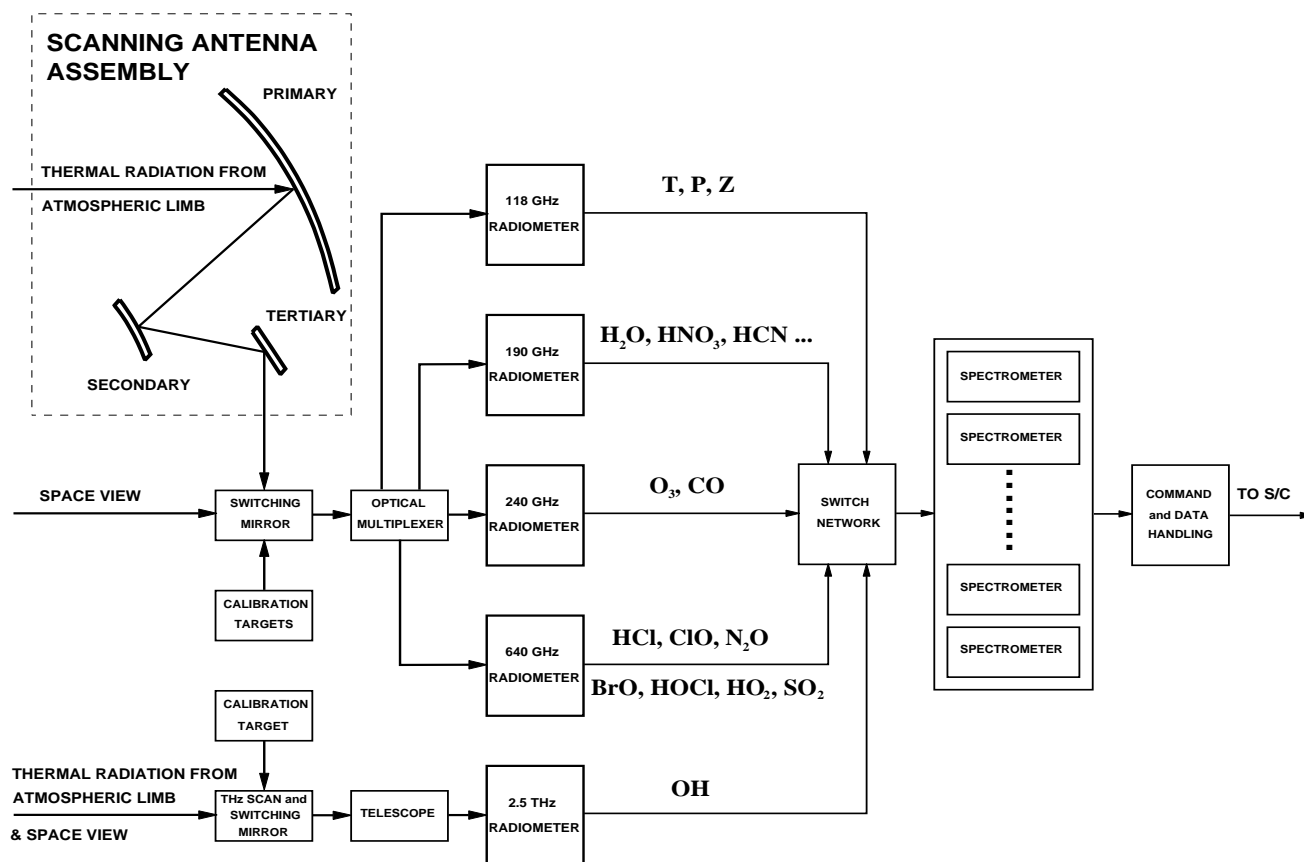


Figure 5-1. EOS MLS signal flow block diagram. D.A. Flower prepared this figure.
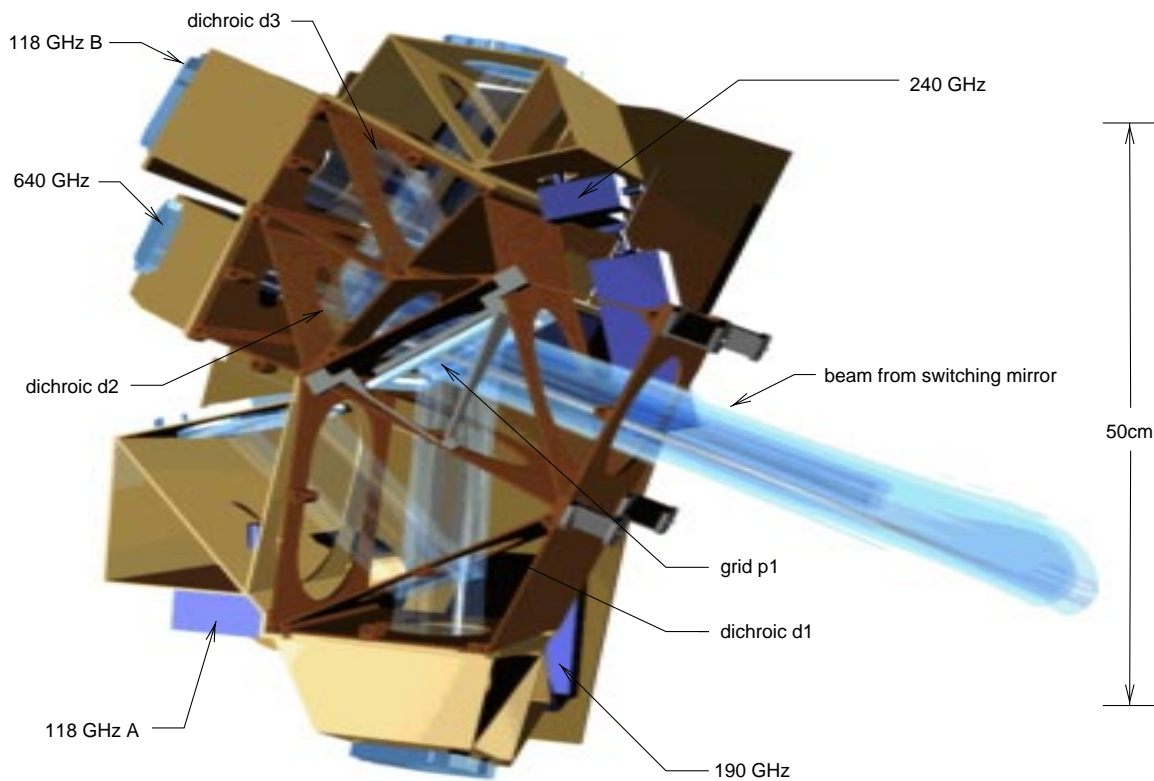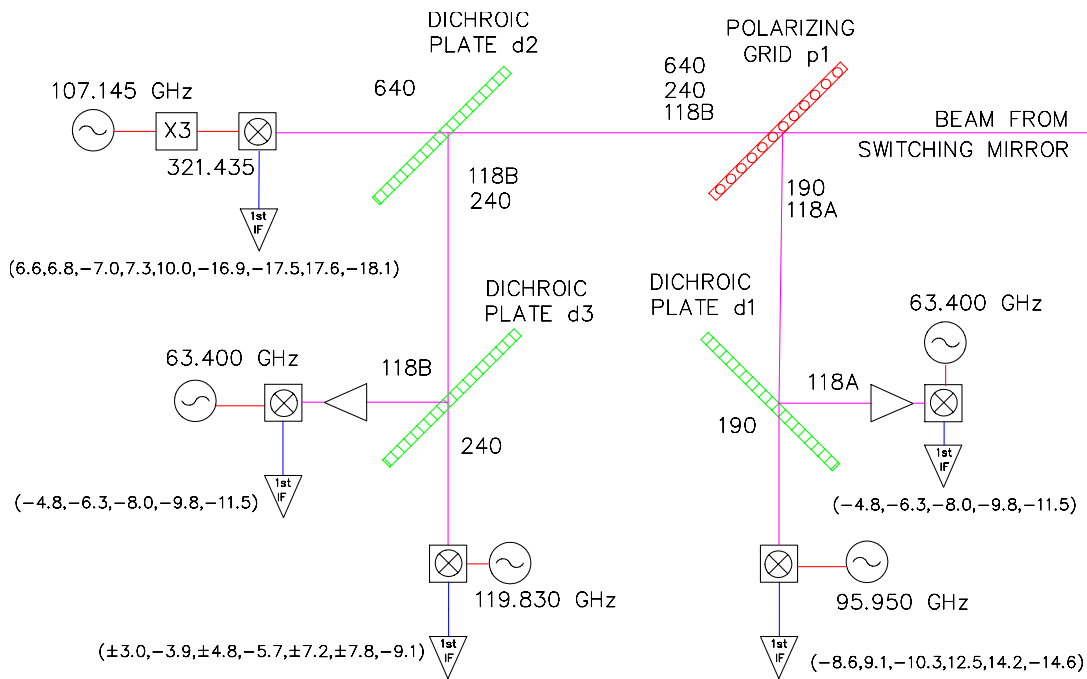
Figure 5-2 (color). Schematic (top) and design (bottom) of the optical multiplexer for the EOS MLS GHz radiometers. The schematic also indicates the fundamental oscillator frequencies (numbers near the circles containing the ~ symbol) used to generate the radiometer local oscillators, and the center IF frequencies (numbers in parentheses) of targeted spectral regions in the radiometer outputs. Amplifiers, up to the first IF stage, are also shown (triangular symbols). R.E. Cofield prepared this figure.

## 5.3  Spectral regions

The spectral regions chosen for measurement by EOS MLS, shown in Figure 5-3, are the result of an extensive investigation to minimize the number of radiometers and spectrometers needed to accomplish the scientific objectives of the experiment, while reliably producing its data products with the required accuracy and resolution.  Figure 5-4, on the following page, shows these regions superimposed on atmospheric signals.
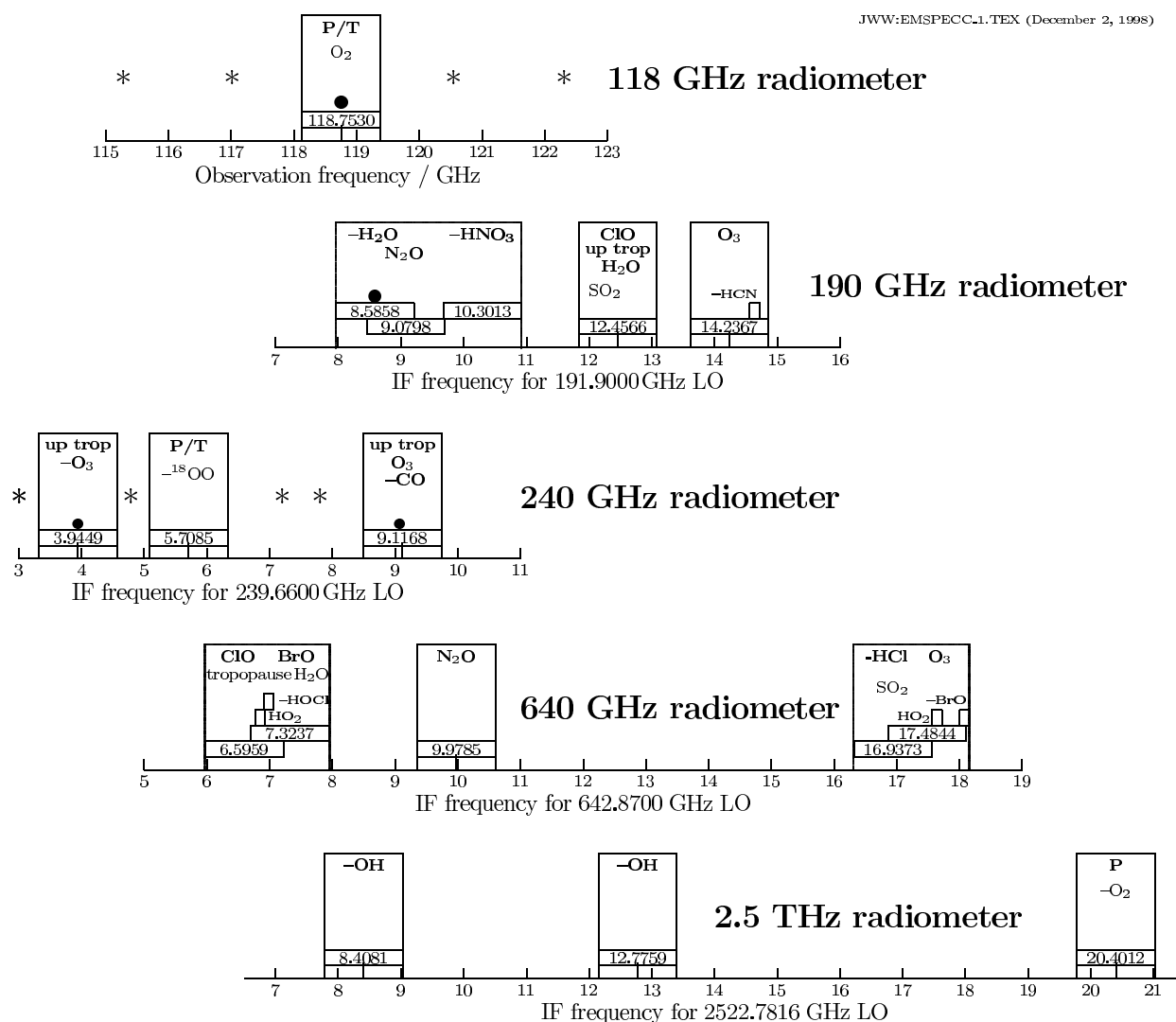


Figure 5-3.  Spectral regions to be measured by EOS MLS.  Each horizontal axis is for a separate radiometer as indicated.  Rectangles with numbers indicate the locations of 'standard' spectrometers, where the number is the frequency at which the spectrometer is centered. Smaller boxes indicate the location of 'mid-band' spectrometers, bullets indicate the location of 'narrowband' spectrometers, and asterisks indicate the location of 0.5 GHz wide individual filters.  The 118 GHz radiometer axis is positioned so that the 118 GHz $O_2$ line coincides with 8.047 GHz IF frequency on the other axes, as is the case for the 126.800 GHz local oscillator of this radiometer.  All radiometers except the 118 GHz are double sideband and receive signals at the indicated IF frequencies above and below the LO frequency.   Some geophysical measurements from each region are indicated.  A minus sign in front of a molecule indicates its signal is observed through the lower sideband of the radiometer.
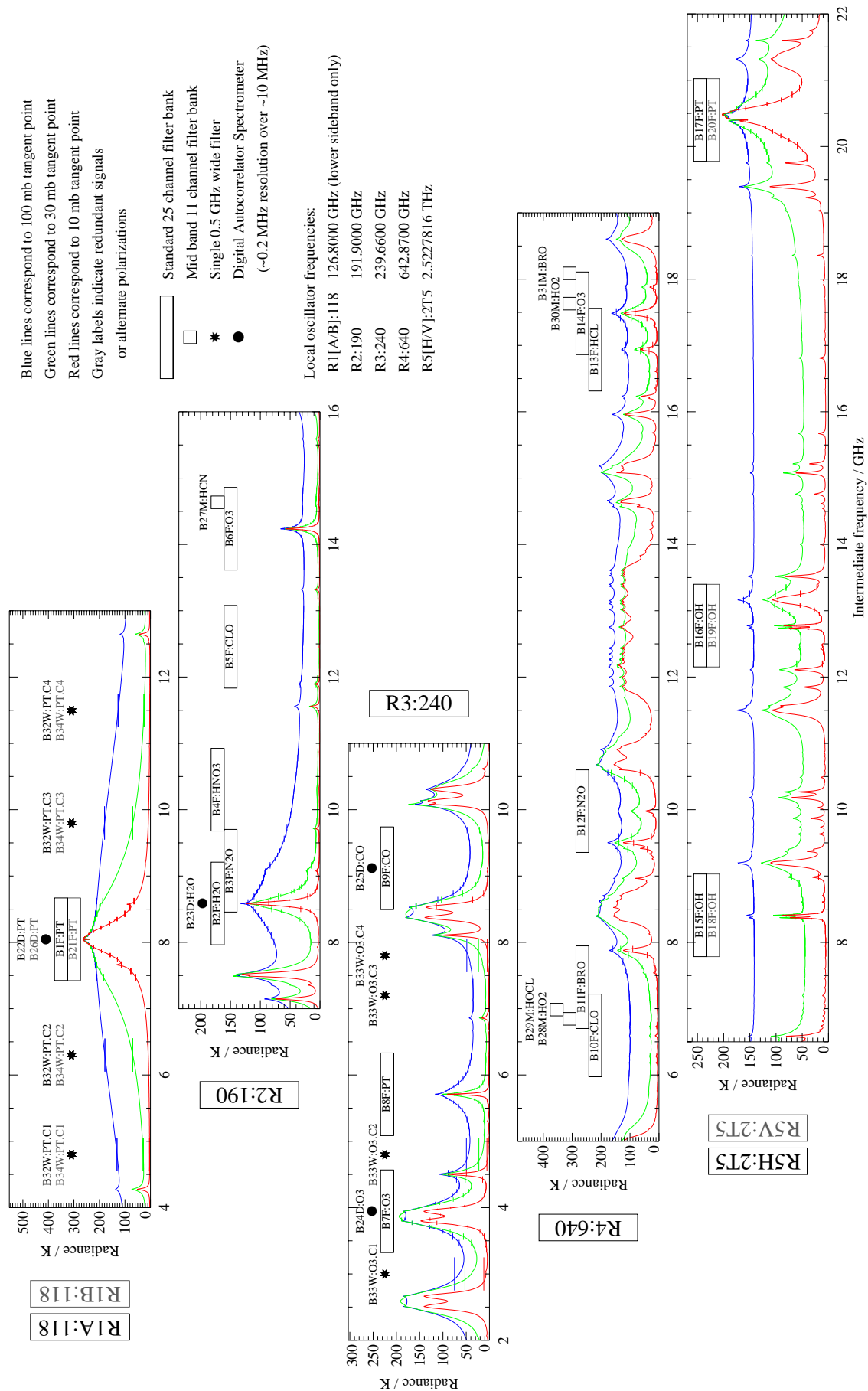
Figure 5-4 (color). Spectral regions measured by EOS MLS, along with atmospheric signals in these regions. N.J. Livesey prepared this figure, taken from Livesey and Wu (1999), using atmospheric signals calculated by M.J. Filipiak. The notation used to designate EOS MLS radiometers and spectral bands is described in Appendix E of Livesey and Wu (1999).
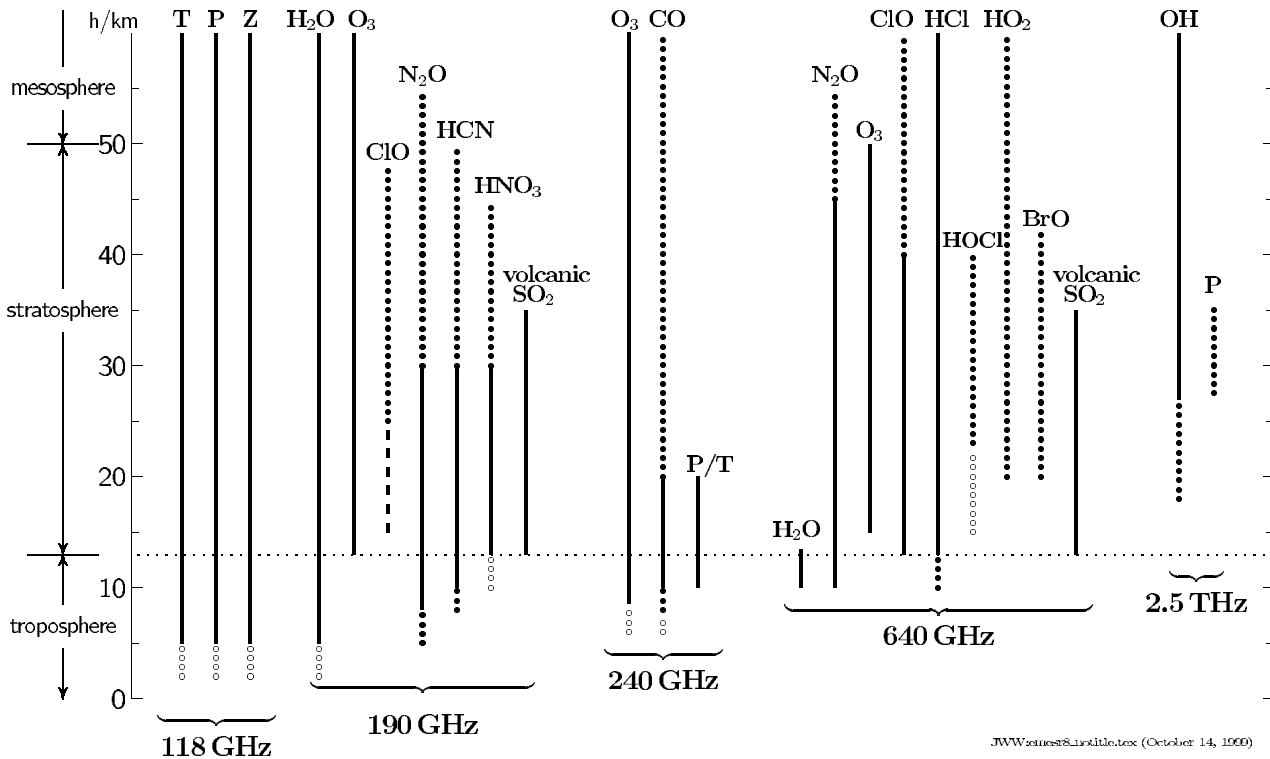
Figure 5-5. Geophysical measurements by individual EOS MLS radiometers. Solid lines indicate useful individual profiles and/or daily maps, dotted lines indicate zonal (or other) averages, the dashed line indicates enhanced ClO in the polar winter vortices. Open circles are goals for more difficult measurements. Measurements of T, P, Z, $H_2O$, $O_3$, HCl, OH and CO extend higher than the 60 km indicated here. The cirrus ice measurement, not shown here, is obtained from a combination of observations from the 118, 190, 240 and 640 GHz radiometers. The signal from the spacecraft gyroscope is used with 118 GHz pressure (P) measurements to provide geopotential height Z. The 2.5 THz measurement of P provides information on the offset between the pointing references for the THz and GHz field-of-views. This figure is updated from Waters et al. (1999).

Figure 5-5 shows the measurements provided by the individual EOS MLS radiometers.

Table 5-2 (on the following page) gives some specifics for the MLS spectral regions, including frequencies of the targeted spectral lines and the maximum expected radiometer noise in each region. There are separate estimates for the noise in the spectrally-varying component of the calibrated radiance and in the spectrally-averaged component of the radiance, as defined in notes 6 and 7 of Table 5-2. The primary molecule to be observed in each region, its expected typical abundance, the targeted spectral line, and the expected signal intensity are also given.

Most MLS data products are obtained from the spectrally-varying component of the radiance, and different scientific uses for the same data product require different precision, which depends upon the amount of averaging and spectral resolution used in the analyses. The spectrally-averaged component of the radiance is used at the lowest ends of the measurement height range to provide information on temperature, $H_2O$, and cirrus ice.

Any radiometer responses in extraneous spectral regions, which might be converted into signals at the IF frequencies of spectral regions targeted for measurements, will be at least 30 dB lower than for the targeted regions. Any responses of the 240 GHz radiometer within 3 GHz of the 118 GHz $O_2$ line will be at least 40 dB lower than in its targeted regions. This ensures that any unwanted atmospheric signal will contribute less than 0.3 K brightness to the received signal, and limits contamination of the 240 GHz upper tropospheric $O_3$ measurements to less than 0.03 K by the strong 118 GHz $O_2$ line.

Table 5-2. Some specifics for the spectral regions measured by EOS MLS.

| radiometer and LO frequency see note 1 (GHz) | primary targeted molecule | abundance expected see note 2 (vmr) | spectral line frequency see note 3 (GHz) | expected signal intensity see note 2 (K, SSB) | measured spectral region Doppler-shifted center freq see note 4 (GHz) | IF freq (GHz) | meas. by (see note 5) | $T_{sys}$ (K,SSB) | spectrally-varying component ( K, SSB) ΔI for 0.17 s 6 MHz | 96 MHz | 500 MHz | $ΔI_{min}$ |
|---|---|---|---|---|---|---|---|---|---|---|---|---|
| **118 GHz** 126.800 (÷2 = 63.400) | O2 wing | 2.1E-01 |  | 1-300 | 115.3 | -11.5 | d |  |  |  | 0.2 | 0.1 |
|  | O2 wing | 2.1E-01 |  | 1-300 | 117.0 | -9.8 | d |  |  |  | 0.2 | 0.1 |
|  | O2 | 2.1E-01 | *118.7503 | 1-300 | 118.7530 | -8.0470 | a,c | 1500 | 1.5 | 0.4 |  | 0.1 |
|  | O2 wing | 2.1E-01 |  | 1-300 | 120.5 | -6.3 | d |  |  |  | 0.2 | 0.1 |
|  | O2 wing | 2.1E-01 |  | 1-300 | 122.0 | -4.8 | d |  |  |  | 0.2 | 0.1 |
| **190 GHz** 191.900 (÷2 = 95.950) | H2O | 5E-06 | 183.3101 | 1-300 | 183.3142 | -8.5858 | a,c | 4000 | 4 | 1 |  | 0.1 |
|  | N2O | 1E-07 | 200.9753 | 15 | 200.9798 | 9.0798 | a | 4000 | 4 | 1 |  | 0.1 |
|  | HNO3 | 1E-09 | 181.5946 | 5 | 181.5987 | -10.3013 | a | 4000 | 4 | 1 |  | 0.1 |
|  | ClO | 5E-10 | *204.352 | 0.4 | 204.3566 | 12.4566 | a | 4000 | 4 | 1 |  | 0.03 |
|  | O3 | 1E-05 | 206.1320 | 1-100 | 206.1367 | 14.2367 | a | 4000 | 4 | 1 |  | 0.1 |
|  | HCN | 1E-10 | 177.2612 | 0.5 | 177.2652 | -14.6348 | b | 4000 | 4 | 1 |  | 0.1 |
| **240 GHz** 239.660 (÷2 = 119.830) (see note 8) | up trop O3 | 5.0E-08 |  | 0.2 |  | +/- 3.0 | d | 4000 |  |  | 0.4 | 0.1 |
|  | up trop O3 | 5.0E-08 | 235.7098 | 2 | 235.7151 | -3.9449 | a,c | 4000 | 4 | 1 |  | 0.1 |
|  | up trop O3 | 5.0E-08 |  | 0.2 |  | +/- 4.8 | d |  |  |  | 0.4 | 0.1 |
|  | 18OO | 8.0E-04 | 233.9462 | 1-100 | 233.9515 | -5.7085 | a | 4000 | 4 | 1 |  | 0.1 |
|  | up trop O3 | 5.0E-08 |  | 0.2 |  | +/- 7.2 | d |  |  |  | 0.4 | 0.1 |
|  | up trop O3 | 5.0E-08 |  | 0.2 |  | +/- 7.8 | d |  |  |  | 0.4 | 0.1 |
|  | CO | 1.0E-07 | 230.5380 | 1.5 | 230.5432 | -9.1168 | a,c | 4000 | 4 | 1 |  | 0.1 |
| **640 GHz** 642.870 (÷2 and ÷3 = 107.145) | ClO | 5.0E-10 | *649.4512 | 8 | 649.4659 | 6.5959 | a | 12,000 | 12 | 3 |  | 0.1 |
|  | HO2 | 5.0E-10 | 649.7015 | 1 | 649.7162 | 6.8462 | b | 12,000 | 12 | 3 |  | 0.1 |
|  | HOCl | 2.0E-10 | 635.8700 | 0.7 | 635.8844 | -6.9856 | b | 12,000 | 12 | 3 |  | 0.1 |
|  | Br-81-O | 5.0E-12 | *650.179 | 0.1 | 650.1937 | 7.3237 | a | 12,000 | 12 | 3 |  | 0.03 |
|  | N2O | 1.0E-07 | 652.8338 | 80 | 652.8485 | 9.9785 | a | 12,000 | 12 | 3 |  | 0.1 |
|  | HCl | 2.0E-09 | *625.9188 | 50 | 625.9327 | -16.9373 | a | 12,000 | 12 | 3 |  | 0.1 |
|  | O3 | 1.0E-05 | 625.3715 | 1-200 | 625.3856 | -17.4844 | a | 12,000 | 12 | 3 |  | 0.1 |
|  | HO2 | 5.0E-10 | 660.4857 | 1 | 660.5006 | 17.6306 | b | 12,000 | 12 | 3 |  | 0.1 |
|  | Br-81-O | 5.0E-12 | *624.768 | 0.1 | 624.7821 | -18.0879 | b | 12,000 | 12 | 3 |  | 0.03 |
| **2.5 THz** 2522.7816 (see note 9) | OH | 5.0E-13 to | *2514.3167 | 0.2-100 | 2514.3735 | -8.4081 | a | 30,000 | 30 | 8 |  | 0.05 |
|  | OH | 1.0E-09 | *2509.9490 | 0.2-100 | 2510.0057 | -12.7759 | a | 30,000 | 30 | 8 |  | 0.05 |
|  | O2 | 2.1E-01 | *2502.3239 | 1-300 | 2502.3804 | -20.4012 | a | 90,000 | 90 | 25 |  | 0.1 |

Note 1: The 118 GHz and 2.5 THz local oscillator (LO) frequencies were selected from engineering considerations; others were chosen to provide atmospheric measurements from both the lower and upper sidebands. The 118 GHz radiometer is single sideband and all others are double sideband. The '(÷ 2 = $f$)' below the local oscillator frequency gives the frequency $f$ of the fundamental oscillator used to generate the LO. There is an additional ÷ 3 for the 640 GHz radiometer because a frequency-tripler is also used there, as well as its mixer being subharmonically pumped like the 118, 190 and 240 GHz radiometers.

Note 2: Values here are typical of what is expected over certain vertical ranges to be covered by MLS; 'vmr' is volume mixing ratio.

Note 3: Spectral lines having fine structure are marked by *.

Note 4: Doppler-shifted values are for MLS looking forward in 700 km orbit. A negative number in the 'IF freq' column indicates the spectral line is in the radiometer lower sideband; ± indicates signals from the targeted molecule are in both upper and lower sidebands.

Note 5: Letters in this column refer to the spectrometers or filters which will be used for measurements in the indicated spectral region: 'a' indicates a 'standard' spectrometer, 'b' indicates a 'midband' spectrometer, 'c' indicates a 'narrowband' spectrometer, and 'd' indicates a 500 MHz wide individual filter. These are described in section 5.4 of this document.

Note 6: The expected 1σ noise in the spectrally-varying component of the radiance (single sideband, after calibration, measured from one channel or filter to another throughout a given radiometer) is the greater of $ΔI_{min}/3$ or $T_{sys}/sqrt(Bτ)$, where $ΔI_{min}$ and $T_{sys}$ are given in the table above, B is the noise bandwidth, and τ is integration time for which the measurement is accumulated. $ΔI_{min}$ is the minimum signal to be measured. The value of τ can range from 0.17 s ( a single instrument integration time) to 1 hour (the integration time for producing monthly zonal means with 5 km vertical and 5° latitude resolution). This noise limit, and range of τ, applies to the accumulation of measurements from different limb scans, all of which are made within the same 0.03° angular (~1.5 km vertical) scan range. Values of the expected radiometric noise for the individual 0.17 s integration time are given in the columns labeled 'Δl for 0.17 s' (at 6 and 96 MHz bandwidths for regions measured by standard and midband spectrometers, and at 500 MHz bandwidth for regions measured by individual filters). All values are in single-sideband units.

Note 7. The expected 1σ noise in the spectrally-averaged component of the radiance from each radiometer (single sideband, after calibration, average value over all channels of the radiometer) measured in an individual 0.17 s integration period is $4×10^{-4} × T_{sys}$ for the 118, 190, 240 and 640 GHz radiometers and $2×10^{-3} ×T_{sys}$ for the 2.5 THz radiometer.

Note 8. Although the 240 GHz radiometer is primarily for upper tropospheric $O_3$, it also provides stratospheric and mesospheric $O_3$.

Note 9: Measurements in both polarizations are averaged to reduce the noise during retrievals of OH.
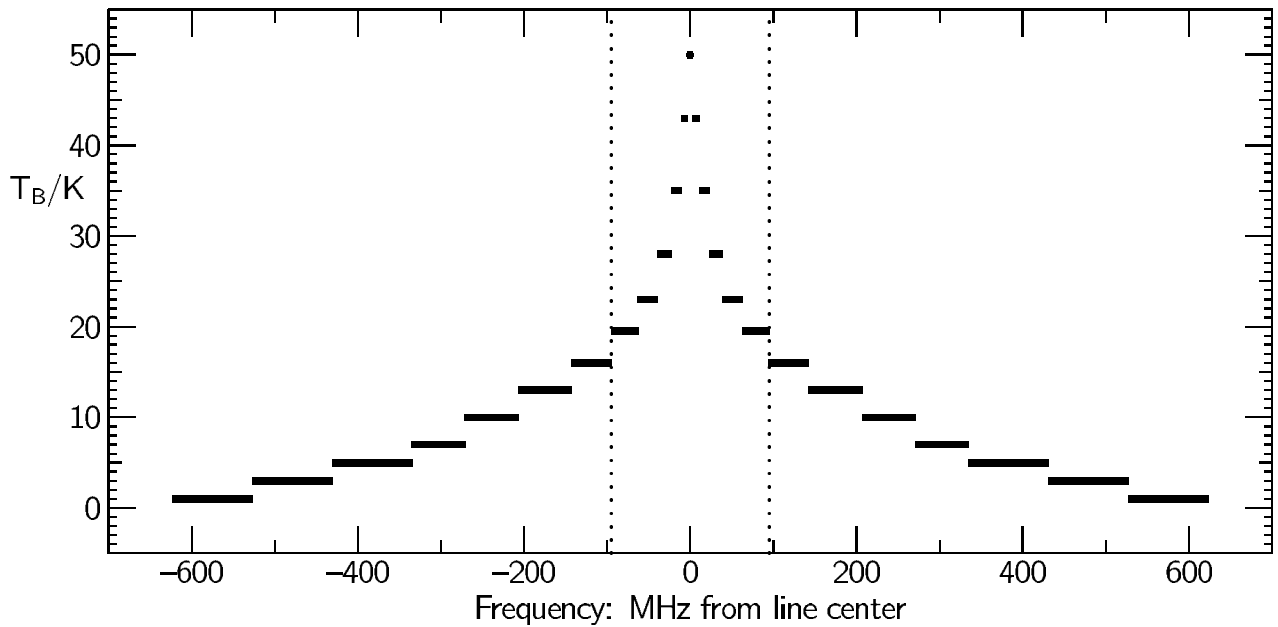
Figure 5-6. Coverage of the EOS MLS 'standard' 25-channel spectrometer. Each filter in the spectrometer is shown as a horizontal bar whose width gives the filter resolution. The 11 filters located between the dotted vertical lines also occur in the EOS MLS 'mid-band' spectrometers. The signal illustrated here is the 206 GHz $O_3$ line shown earlier in Figure 3-3 measured by UARS MLS, and extended outward to the broader spectral coverage of EOS MLS.

## 5.4 Spectrometers

Spectrometers with different spectral resolutions and bandwidths are used to cover the different altitude ranges for which measurements are needed. Measurements at lower altitudes require more spectral coverage, but less resolution, than do measurements at higher altitudes. Four types of spectrometers are used in EOS MLS.

'Standard' 25-channel spectrometers are the primary source of information for measurements throughout the stratosphere (atmospheric pressure range from ~100 to ~1 hPa) which require spectral coverage of ~1300 MHz at the lower altitudes and resolution of ~6 MHz at the higher altitudes, as can be seen from Figure 3-3. The spectral regions indicated by 'a' in the 'meas. by' column of Table 5-2 use these spectrometers; the regions are also illustrated earlier in Figures 5-3 and 5-4. Individual channel positions (frequency relative to the down-converted frequency of the measured spectral line) and widths (full width between the half-power points of the channel response) for these spectrometers are given in Table 5-3, and illustrated in Figure 5-6.

Table 5-3. Positions (relative to spectral line center) and widths (full widths between half power points) of channels in the 'standard' 25-channel spectrometers. Values for channels 8 to 18 also apply to the 'mid-band' spectrometers.

| channel number | position (MHz) | width (MHz) | channel number | position (MHz) | width (MHz) | channel number | position (MHz) | width (MHz) |
|---|---|---|---|---|---|---|---|---|
| 1 | -575 | 96 | 8 | -79 | 32 | 19 | 119 | 48 |
| 2 | -479 | 96 | 9 | -51 | 24 | 20 | 175 | 64 |
| 3 | -383 | 96 | 10 | -31 | 16 | 21 | 239 | 64 |
| 4 | -303 | 64 | 11 | -17 | 12 | 22 | 303 | 64 |
| 5 | -239 | 64 | 12 | -7 | 8 | 23 | 383 | 96 |
| 6 | -175 | 64 | 13 | 0 | 6 | 24 | 479 | 96 |
| 7 | -119 | 48 | 14 | 7 | 8 | 25 | 575 | 96 |
| | | | 15 | 17 | 12 | | | |
| | | | 16 | 31 | 16 | | | |
| | | | 17 | 51 | 24 | | | |
| | | | 18 | 79 | 32 | | | |

'Midband' spectrometers, consisting of the center 11 channels (numbered 8 to 18) in Table 5-3, are used for additional measurements in the middle and upper stratosphere (atmospheric pressures from ~10 to ~1 hPa). The spectral regions using these spectrometers are indicated by 'b' in the 'meas. by' column of Table 5-2, and illustrated in Figures 5-3 and 5-4 occurring earlier in this document. Locations of individual filters in these spectrometers are also shown in Figure 5-6.

'Narrowband' spectrometers provide mesospheric measurements. These have a 10 MHz spectral width and resolution of 0.2 MHz to cover narrow spectral lines at atmospheric pressures below ~1 hPa (see Figure 3-3). They are used in spectral regions indicated by 'c' in the 'meas. by' column of Table 5-2 (and illustrated in Figures 5-3 and 5-4 occurring earlier in this document) to provide mesospheric measurements of temperature, $H_2O$, $O_3$ and CO. These spectrometers will be implemented as digital autocorrelators. The 'standard' spectrometers provide adequate spectral resolution for the mesospheric OH signals that have a Doppler-broadened halfwidth of ~3 MHz (see Figure 3-3) which is well matched to the 6 MHz resolution of the center channels of the standard spectrometers.

'Individual filters', 0.5 GHz wide, extend the spectral range of the 25-channel spectrometers for measurements extending down into the troposphere. These filters are at spectral locations indicated by 'd' in the 'meas. by' column of Table 5-2, and are illustrated in Figures 5-3 and 5-4 occurring earlier in this document.

The instrument contains a total of 19 'standard' spectrometers, 5 'mid-band' spectrometers, 4 'narrowband' autocorrelator spectrometers, and 12 'individual' filters (there are 4 individual filters in both the primary and redundant 118 GHz radiometers).

The position and width of each channel will be known to within 10% of the full width between half power points. This ensures that the channel position and resolution are within an acceptable range for gathering the needed information. The fraction of spectrally-flat input power received within each channel's width will be 0.85 or greater, with 0.90 as a goal. This ensures that signals received by each filter arise mainly from the targeted region.

The frequency stability of channel responses (at frequencies of the maximum response and the –10 dB points on the edges), including cumulative effects of all down-conversions except that of the first local oscillator for the 2.5 THz radiometer, will be better than 0.01 MHz over time periods up to 1 minute. This ensures that frequency shifts of the channel response over an individual limb scan are less than 10% of the spectral line Doppler width for the GHz channels, and less than the Doppler width for the 2.5 THz channels. The requirement on the GHz channels is tighter because the Doppler shift of atmospheric spectral lines will be determined during analyses of data from certain of these channels. The local oscillator frequency for the 2.5 THz bands can slowly drift over a range of approximately ± 2 MHz, and will be a free parameter determined during ground data processing.

Over time periods from 1 minute up to the life of the instrument, either the frequency stability, or knowledge of drifts in frequency of the channel responses, will be better than 0.5% of the channel width for the GHz bands, including cumulative effects of all down-conversions. This ensures that long-term drifts will not significantly degrade the quality of geophysical measurements retrieved from the data. The same specification applies to the THz bands but without including the effects of frequency down-conversion from the first local oscillator since those effects will be accounted for during data processing.

## 5.5  Field-of-view (FOV)

The beamwidths, beam efficiencies, and placement and coincidences of the field-of-view boresights are important design parameters for the EOS MLS instrument.

'FOV beamwidth' is defined as the angle between the half-power points of the antenna response. 'Beam efficiency' is defined as that fraction of power from an isotropic source which is collected within a specified angular range centered at the antenna boresight. The MLS FOV beamwidths and beam efficiency are set by the vertical resolution needed for the measurements.  The values chosen are an acceptable compromise between the scientific desire for better vertical resolution, and the engineering/accommodation difficulties associated with the increase in antenna size required for better resolution.  They correspond to an antenna for the GHz channels which is the same size as that used for the UARS MLS, but the shorter-wavelength EOS MLS measurements provide better vertical resolution than UARS MLS.

The EOS MLS FOV beamwidths are given in Table 5-4.  The beam efficiency within an angular range of 2.5 times the beamwidth is 0.95 or greater.

Table 5-4.  EOS MLS field-of-view beamwidths (full width between half-power points)

| Radiometer | FOV beamwidth in vertical plane at the limb tangent point | FOV beamwidth in horizontal plane at the limb tangent point |
|---|---|---|
| 118 GHz | 6.5 km | 13 km |
| 190 GHz | 4.5 km | 9 km |
| 240 GHz | 3.5 km | 7 km |
| 640 GHz | 1.5 km | 3 km |
| 2.5 THz | 2.5 km | 2.5 km |

The angular pattern of the EOS MLS FOV response will be similar to that for UARS MLS, whose measured 205 GHz response is shown in Figure 5-7 on the following page.  The noise floor on the measurements shown in Figure 5-7 is ~74 dB ($4\times10^{-8}$) below the peak boresight value of the response.

'FOV boresight' is defined as the direction given by the peak value of the Gaussian function which best fits the antenna response down to the -10 dB power points.  FOV boresights of the 190, 240 and 640 GHz radiometers coincide with the 118 GHz FOV boresight to within one-fifth of the 118 GHz beamwidth.  Direction of the 2.5 THz FOV boresight relative to the direction of the 118 GHz FOV boresight will be known to within one-fifth of the 118 GHz beamwidth.  The scan plane of the 2.5 THz boresight is within 10 km of that of the 118 GHz boresight at the atmospheric limb tangent point, over the tangent height range of 10 to 60 km, and the THz and GHz scans are synchronized to within one individual instrument integration period.

To ensure efficient coverage of the vertical region of interest, the accuracy in placement of the tangent height of the FOV boresights, after in-orbit adjustments, will be ±0.5 km at the start of each limb scan (which can degrade to ±1 km at the end of the limb scan).  The tangent heights are with respect to a geoid model of the Earth and the scan accounts for Earth's oblateness.
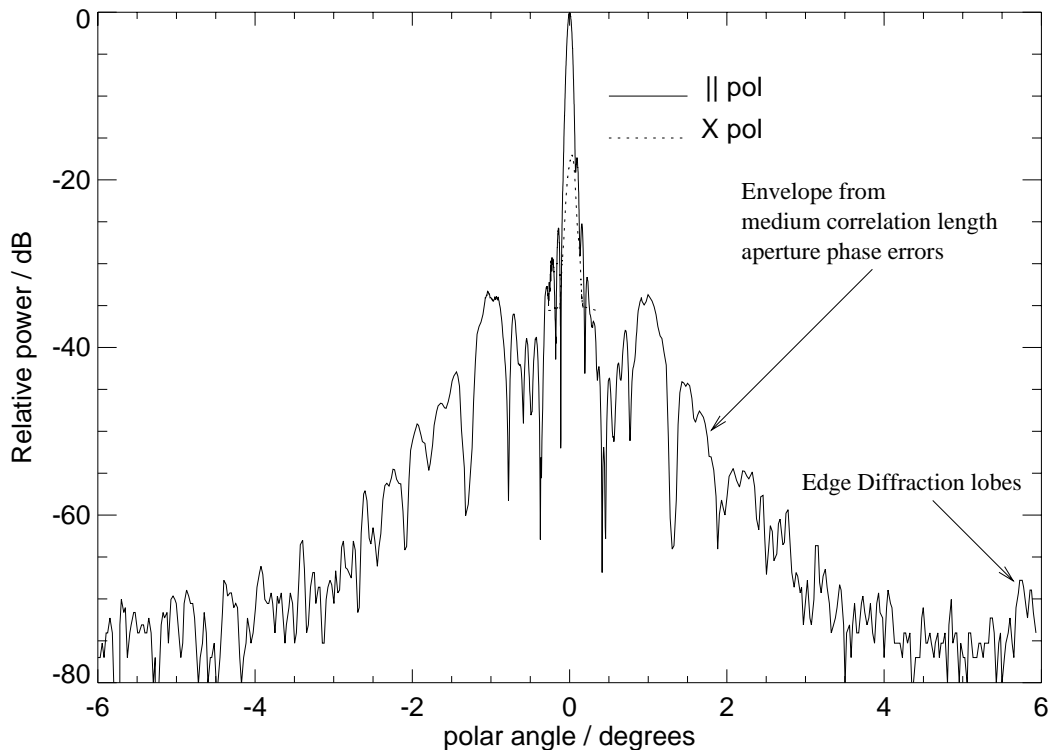
Figure 5-7.  The measured UARS MLS field-of-view response at 205 GHz.  This shows a 'cut' of the response along the vertical direction projected at the limb tangent point.  Note the vertical scale is in decibels.  The response to atmospheric radiation polarized parallel (‖ pol) to the polarization of the radiometer is indicated by the solid curve, and that polarized perpendicular (× pol) to that of the radiometer is indicated by the dashed curve.  EOS MLS field-of-view patterns will be similar to that shown here.  R.E. Cofield prepared this figure.

To ensure that tangent height uncertainties due to boresight elevation uncertainties are comparable to, or less than, the equivalent height uncertainties in MLS measurements of tangent pressure, the change in elevation of the FOV boresights with respect to nadir during each limb scan will be known to an accuracy of 2 arcsecond ($3\sigma$), and the rate of change will be known to an accuracy of 1 arcsecond per second ($3\sigma$), at time scales between 0.17 and 25 seconds.  (Note: 1 arcsecond corresponds to 15 m vertical distance at the limb tangent point.)  MLS instrument data on the FOV boresight elevation is recorded twice per individual radiometric integration period, and spacecraft data relevant to the MLS FOV boresight elevation is recorded at least once per individual radiometric integration period.  Jitter in the FOV boresights at time scales shorter than 0.17 second will not exceed 2 arcsecond ($3\sigma$).

The absolute pointing knowledge required for EOS MLS geopotential height measurements will be obtained from the CHEM satellite star tracker and gyroscope data.  Drifts in these data will be 'calibrated out' by analyses of overlapping observations from successive orbits in the polar regions (see Figure 6-1, later in this document), and in the tropics where MLS temperature data indicate stable atmospheric conditions.  Preliminary analyses indicate that pointing knowledge of 2 arcseconds ($3\sigma$) accuracy throughout the orbit can be maintained by this process.  Biases in pointing will also be checked and corrected by occasional comparison of geopotential height retrieved from MLS with geopotential height fields from operational meteorological data.  Comparisons will also be made with overlapping HIRDLS geopotential height retrievals to remove biases.  HIRDLS can remove drifts in satellite pointing errors much more effectively than MLS because the HIRDLS azimuth scanning capability allows comparison *throughout the orbit* of measurements from adjacent orbits.
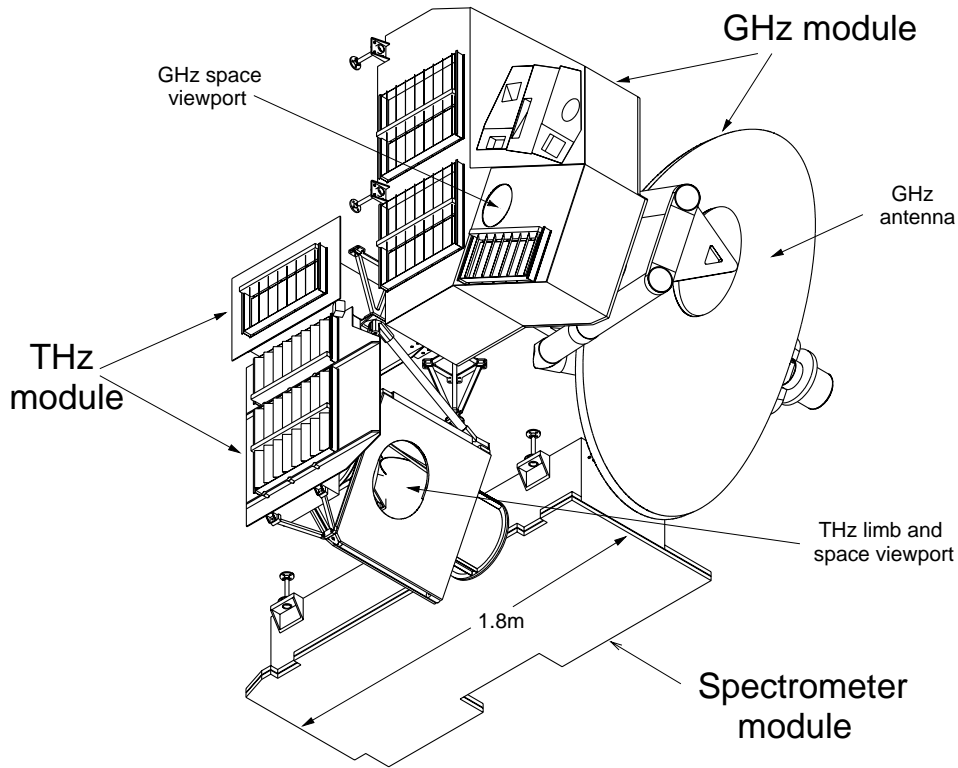
Figure 5-8.  The EOS MLS instrument.  The three modules are separately mounted to the CHEM satellite with the approximate relative locations and orientations shown here.  The EOS MLS instrument design team prepared this figure.

## 5.6  Overall instrument

Figure 5-8 shows a sketch of the overall EOS MLS instrument.  It has three major modules:

1. the 'GHz module' which contains the GHz antenna system, calibration targets, switching mirror, optical multiplexer and radiometers for the 118, 190, 240 and 640 GHz measurements,
2. the 'THz module' which contains the THz scan and switching mirror, calibration target, telescope and radiometers at both polarizations for the 2.5 THz measurements,
3. the 'Spectrometer Module' which contains the spectrometers, command and data handling, and power distribution systems.

Table 5-5 gives best estimates of the mass, full-up power (average power over two orbits) and data rate for the overall instrument as presented at the September 1999 MLS Critical Design Review (CDR) - and the allocations to MLS.  Although the CDR best estimates for all parameters are well within the allocations, the estimate for full-up power does not have the 10% margin that is programmatically-required at this stage of instrument development.  Section 5.8, later in this document, gives a scenario for time-sharing measurements if needed to reduce power consumption.

Table 5-5.  CDR best estimates and allocations for the overall mass, full-up average power, and data rate.

| parameter | best estimates given at Sept 1999 MLS CDR | allocations as of Sept 1999 |
|---|---|---|
| mass | 442 kg | 490 kg |
| power | 531 Watts | 550 Watts |
| data rate | 98.3 kilobits /second | 100 kilobits/second |

## 5.7 Calibration

There are four categories of calibration for the EOS MLS instrument.

1. 'Radiometric calibration' gives the absolute power incident upon the antenna that is received in each spectral channel. As is typical in microwave radiometry, this power is calibrated in terms of a 'temperature' that is proportional to the amount of power received, and converges - in the long-wavelength (Rayleigh-Jeans) limit - to the absolute temperature of a blackbody emitting that amount of power. The calibrated outputs are referred to as 'radiances'.

2. 'Field-of view (FOV) calibration' gives the response of the instrument to the input signal as a function of the angle at which the signal is incident upon the antenna.

3. 'Spectral calibration' gives the relative response of the instrument to the input signal as a function of the frequency of the signal.

4. 'Engineering calibration' gives the output of engineering sensors in appropriate units (e.g., volts, amperes).

Instrument calibration is performed in each of these categories. Examples of pre-launch calibration are: (1) measurement of the emissivities of the on-board targets and the loss in the antenna for radiometric calibration, (2) end-to-end measurement of the antenna response as a function of angle, or of the position of a probe in the antenna aperture near-field, for FOV calibration, (3) end-to-end measurement of the frequency response of each channel (including responses in radiometer sidebands) for spectral calibration, and (4) calibration of engineering sensors against accepted standards. In-orbit calibration includes (1) observations of the on-board targets and 'cold space' between each limb scan for radiometric calibration, (2) occasional scans of the moon for FOV calibration, and (3) occasional frequency-sweeps with an on-board signal source for frequency calibration. Consistency of the measured spectral line shapes (as a function of tangent point pressure) with those calculated from a radiance 'forward model' also provides an in-orbit test of spectral and field-of-view calibration.

Radiometric calibration parameters are used primarily in MLS Level 1 data processing. Spectral and field-of-view calibration parameters are used primarily in Level 2 data processing. (See section 7 of this document, and references given there, for a description of MLS data processing.)

Specifications on the radiometric, spectral and field-of-view calibration accuracy are as follows.

1. Radiometric calibration. The systematic uncertainty in the atmospheric/Earth radiances measured through each spectral channel shall be less than:

   (a) 3K (at the 90% confidence level) for the <u>absolute value</u> of the radiances

   (b) 1% or $\Delta I_{min}/3$ for the <u>spectrally-varying component</u> of the radiances measured from one channel or filter to another throughout a given radiometer (where $\Delta I_{min}$ for each spectral region is given in Table 5-2, and represents the smallest signal to be measured).

2. Spectral and field-of-view calibration. The spectral and FOV responses shall be characterized sufficiently that their separate uncertainties do not introduce uncertainties in the MLS 'forward model' calculations of the atmospheric/Earth radiances of more than (at the 90% confidence level):

   (a) 3 K in the <u>absolute value</u> of radiances measured through each spectral channel, and

   (b) 1% or $\Delta I_{min}/3$ for the <u>spectrally-varying component</u> of the radiances measured from one channel or filter to another throughout a given radiometer (where $\Delta I_{min}$ for each spectral region is given in Table 5-2, and represents the smallest signal to be measured).

All MLS calibration is traceable to fundamental standards.

Methods for calibrating EOS MLS will be similar to those used for UARS MLS (Jarnot et al. 1996). The major difference will be in field-of-view calibration where compact range and/or near-field techniques will be used for EOS MLS.

## 5.8 Measurement time sharing (if needed)

It is extremely desirable that all EOS MLS measurements be performed continuously and simultaneously. The critical design review estimates of average overall power consumption for full-up continuous operation are well within the MLS allocations, as mentioned earlier in section 5.6. However, this estimate does not have the 10% margin that is programmatically-required at CDR stage of instrument development.

The following logic is used to select two radiometers whose operation could be time-shared and keep overall average power consumption well within the margins required at time of CDR. Switching between these two radiometers would be done on a monthly basis. (Approximately 1 day is needed for settling of switching thermal transients in order achieve stability required for all measurements, but some measurements will be possible in a much shorter time after switching.)

1. The 118 GHz radiometer should not be time-shared because of the 'universal' need for its temperature and pressure measurements.
2. The 190 GHz radiometer should not be time-shared because of the importance of its water vapor (both tropospheric and stratospheric) measurement.
3. This leaves the 240, 640 and 2.5 THz available for time-sharing.
4. The 640 GHz and 2.5 THz radiometers should be on together, at least some of the time, because $HO_2$, ClO, HCl and HOCl from 640 GHz are chemically-related to (and should be measured simultaneously with) OH from the 2.5 THz.
5. This leaves time-sharing of 240 GHz with either 640 GHz or 2.5 THz
6. It is better to have the 640 GHz on continuously than 2.5 THz because (a) the 640 GHz provides a large number of measurements and has the best vertical resolution of any EOS MLS radiometer, and (b) every-other-month measurements of stratospheric OH are, at the current time, thought to be adequate.
7. This leaves time-sharing of the 240 GHz and 2.5 THz radiometers, and the two operation modes given in Table 5-6.

The required time-sharing of measurements, if any, needed to meet power allocations will be further addressed as the instrument design matures and the required power margin decreases. The instrument design has reasonable flexibility for accommodating changes in time-sharing modes.

Table 5-6. Two operational modes for time-sharing to reduce MLS power consumption.

| mode | operational status of radiometers | measurements lost in this mode |
|---|---|---|
| 1 | 2.5 THz radiometer off, all other radiometers on | stratospheric OH |
| 2 | 240 GHz radiometer off, all other radiometers on | upper tropospheric ozone, CO (note: stratospheric ozone is measured) |

# 6. Measurement Coverage

The EOS CHEM orbit is sun-synchronous at 705 km altitude with 98$^o$ inclination and 1:45 p.m. ascending equator-crossing time. MLS performs observations with the instrument fields-of-view scanning the limb *in the orbit plane* to provide 82$^o$ N to 82$^o$ S latitude coverage on each orbit.

The limb scans for nominal operation are synchronized to the orbit (using the node-crossing signal from the spacecraft), with the number of scans per orbit an integer multiple of 4, and phased such that limb scan locations occur over the equator. This gives the same latitude sampling in the northern and southern hemispheres, and on the ascending and descending portions of the orbit. MLS nominal operations have 240 limb scans per orbit to give 1.5$^o$ (165 km) along-track separation between adjacent limb scans; this separation is well-matched to the along-track resolution expected for upper tropospheric water vapor measurements. Figure 6-1 shows the locations of measurements with this scan pattern for one 24-hour period.
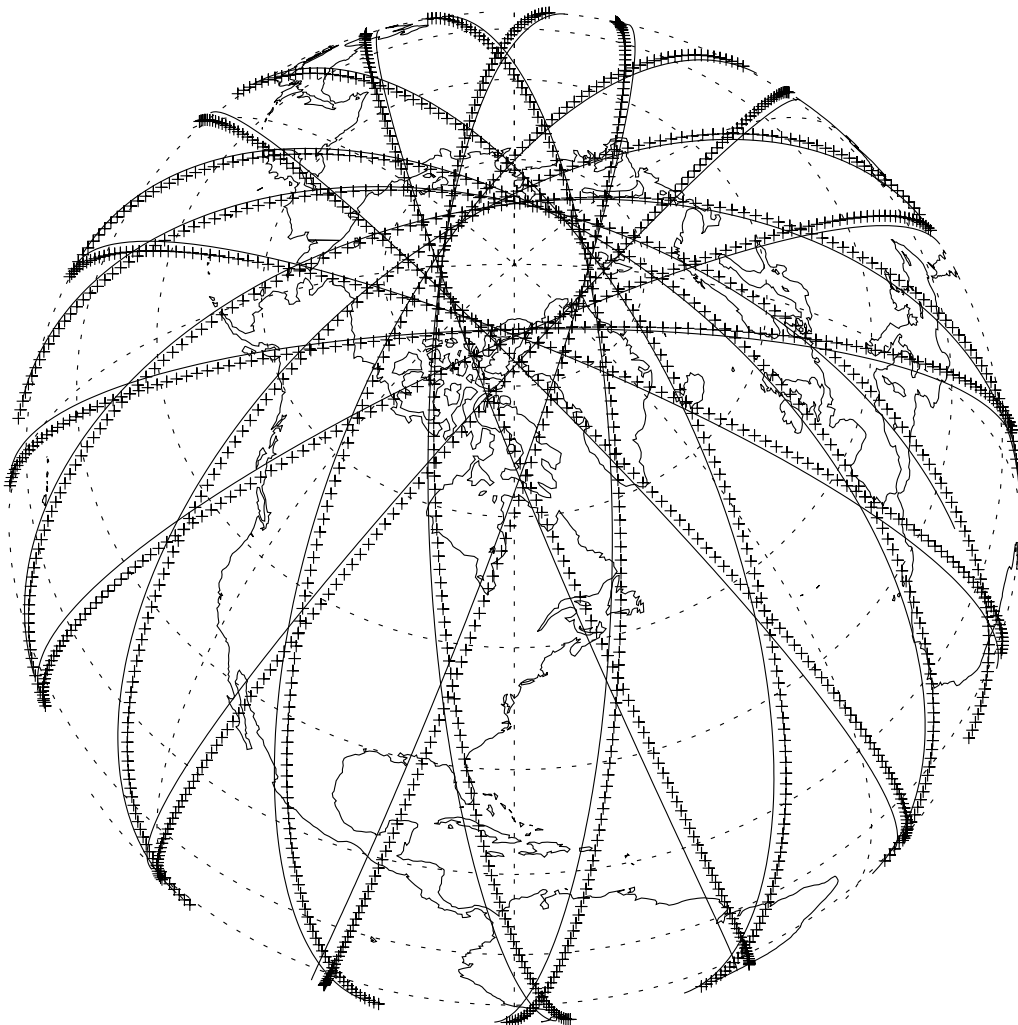


Figure 6-1. EOS MLS measurement locations for a 24 hour period. Each cross gives the location of the tangent points for individual limb scans. The continuous line is the suborbital track, which is slightly displaced from the tangent points because of Earth's rotation during the time in which the satellite moves forward to the tangent point latitude. The ascending portions of the orbit are those with the southeast-northwest tilt. Daily coverage at high latitudes in the Southern Hemisphere is analogous to that of the Northern Hemisphere shown here. R.R. Lay prepared this figure.
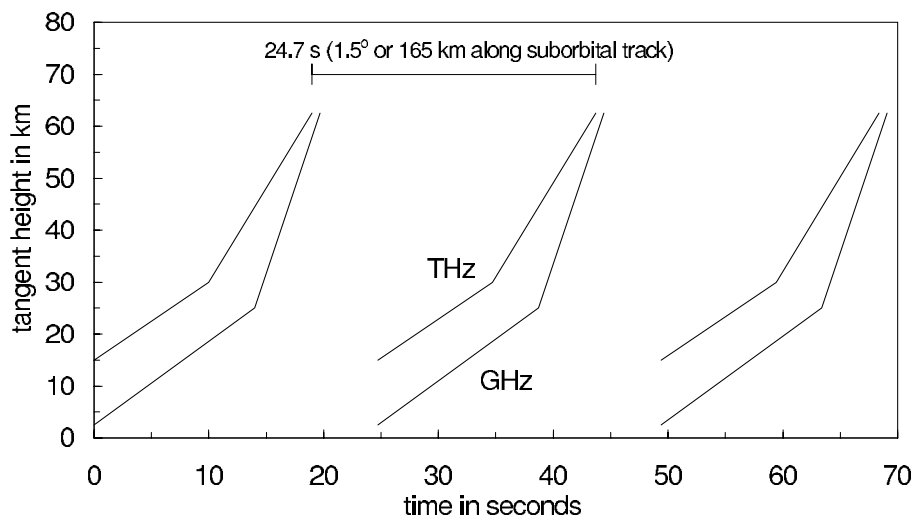
Figure 6-2. EOS MLS nominal operational scan. The curves give the height, at the tangent point, of the FOV boresight as a function of time. Radiometric calibration (observation of blackbody target and of cold space) and mirror retrace are performed during each gap. The scan is in the upward direction from lower to higher heights, causing the tangent point loci to be more vertical when plotted as a function of horizontal distance, as discussed in the text and shown in Figure 6-3 on the following page. The ~1 s difference between the end times of the THz and GHz scans is to reduce peak power drawn from the spacecraft when mirrors are moved more quickly through a larger angular range following the end of the limb scan.

The nominal profile for individual limb scans is shown in Figure 6-2, and has repeat period (24.7 s) which is 1/240th of the orbital period. The scan range is 15 to 62.5 km for the THz radiometer, and 2.5 to 62.5 km for the GHz radiometers which provide measurements to lower altitudes in the troposphere. This scan spends more time in the lower stratosphere and, for the GHz radiometers, in the upper troposphere, to emphasize these atmospheric regions which are currently of great scientific interest. The scan will be performed continuously (i.e., non-stepped), and the 1/6 s instrument integration time provides radiance measurements every ~0.3 km in the vertical in the upper troposphere and lower stratosphere and every ~1 km in the middle and upper stratosphere. Alternative scan programs will be used occasionally to provide measurements at higher altitudes in the mesosphere and (for some measurements) in the lower thermosphere.

MLS observes in the *forward* direction (direction of orbital motion), and the limb is scanned in an *upward* direction to give an observation path tangent point locus which is nearly vertical. The tangent points at greater heights are closer to the satellite, but in the Earth frame of reference this is compensated by the satellite's forward motion. The horizontal deviation of the tangent point locus from a vertical line is approximately ±20 km (tilting forward below ~25 km tangent height, and backward above ~25 km tangent height) over the complete scan range for the nominal scan pattern described above. The observation geometry in the orbit plane is shown in Figure 6-3.

As the EOS CHEM orbit is sun-synchronous (i.e., the orbit plane has a constant orientation relative to the Earth-Sun line), MLS observations at a given latitude on either the ascending (north-going) or descending (south-going) portions of the orbit have the same local solar time throughout the mission as indicated in Figure 6-4. The local solar zenith angle at a given latitude, and the boundaries between the day and night portions of the orbit, vary around an annual cycle as also shown in Figure 6-4.
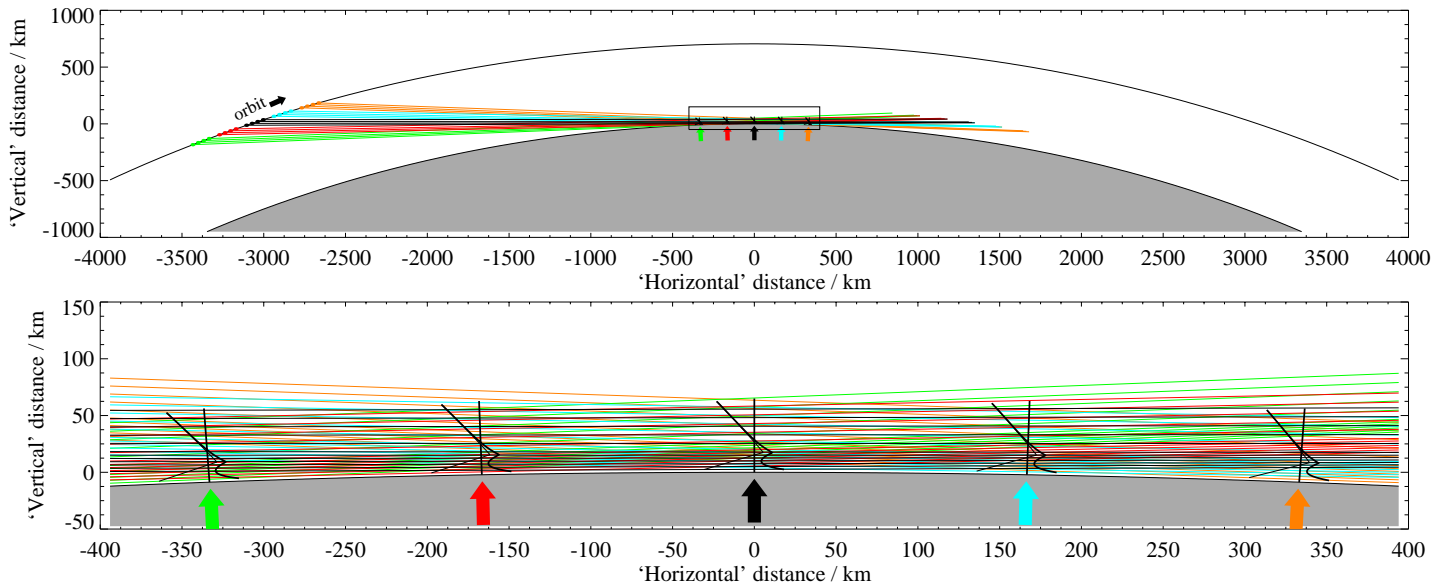
Figure 6-3 (color). The EOS MLS observation geometry in the plane of one orbit. The lower panel gives an expanded portion of the top panel. The MLS line-of-sight paths are the colored/gray lines going mostly horizontal across the figure; only 12 of the 120 limb ray paths for 5 limb scans are shown. Earth's surface is the gray shaded area. The shorter lines extending radially from Earth's surface (indicated by arrows) are the nominal locations of the profiles retrieved from MLS observations. The bent lines, shown with each of the nominal profile locations, are the geometrical loci of the GHz FOV tangent point for the limb scans. The thicker curved lines below ~20 km in the 'vertical' show the loci of the true refracted tangent points. The THz tangent point is displaced forward of the GHz by ~50 km at 15 km tangent height, decreasing to ~5 km at 60 km. From Livesey and Read (1999).
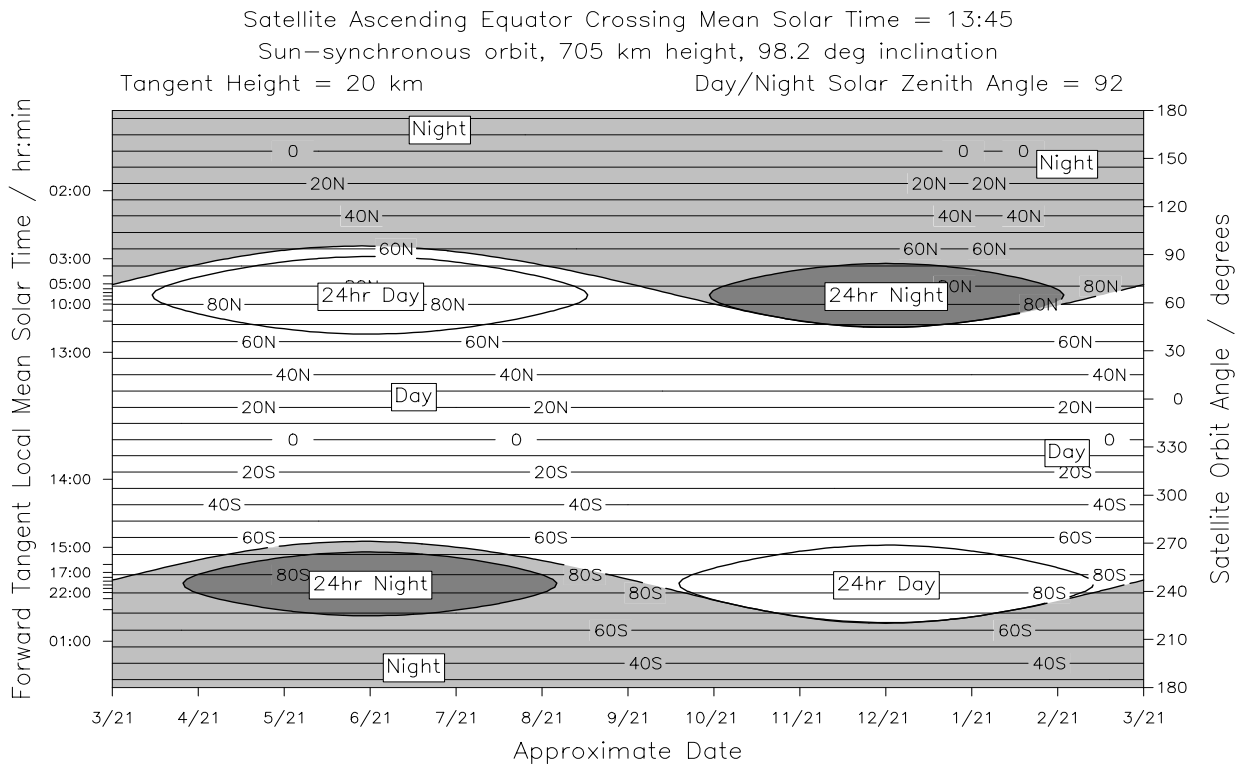


Figure 6-4. Variation, over an annual cycle, of the latitude range where MLS measurements are in day and in night. The horizontal axis gives the approximate date. The right hand vertical axis gives the orbit angle (defined as zero when the satellite is over the equator); the left hand vertical axis gives the corresponding local mean solar time at the (forward) tangent point of MLS observations. Horizontal lines give the latitude of the MLS tangent point, and the day-night boundary is defined as 92° local solar zenith angle. M.J. Filipiak prepared this figure.

# 7. Data Processing

## 7.1 EOS MLS data processing overview

Figure 7-1 gives a top-level flow diagram of the EOS MLS data processing.

Level 1 processing creates the MLS Level 1B calibrated radiances and instrument engineering data. Inputs to this step are: (a) the MLS Level 0 data, which are unprocessed instrument data, (b) the satellite ephemeris and engineering data, which are used, for example, to obtain satellite location and attitude, and (c) solar, lunar and planetary ephemerides, which are used to 'flag' situations when bright objects might be in the MLS fields-of-view.

Level 2 processing creates files of retrieved geophysical parameters at full resolution using the MLS Level 1B data and operational meteorological data as inputs.

Level 3 processing creates files containing (1) gridded daily maps, (2) daily zonal means, (3) gridded monthly average maps, and (4) monthly zonal means. Level 3 data for products which have good signal-to-noise on individual measurements will be produced from the Level 2 data. Level 3 zonal means and monthly maps for 'noisy products' - those with poor or marginal signal-to-noise on individual measurements (such as BrO and lower stratospheric OH) - will be produced directly from the Level 1B radiances.

Summary descriptions of these processing steps are given in following subsections. The EOS MLS data products are described in section 8.

Current plans are for EOS MLS production data processing to be done, under direction of the MLS Science Team, at the MLS Science Investigator-led Processing System (SIPS) implemented by Raytheon ITSS in Pasadena, California. The MLS data will be transferred to the GSFC Distributed Active Archive Center (DAAC) for archive and public distribution.



Figure 7-1. EOS MLS Data Processing Flow.

## 7.2 Level 1 data processing

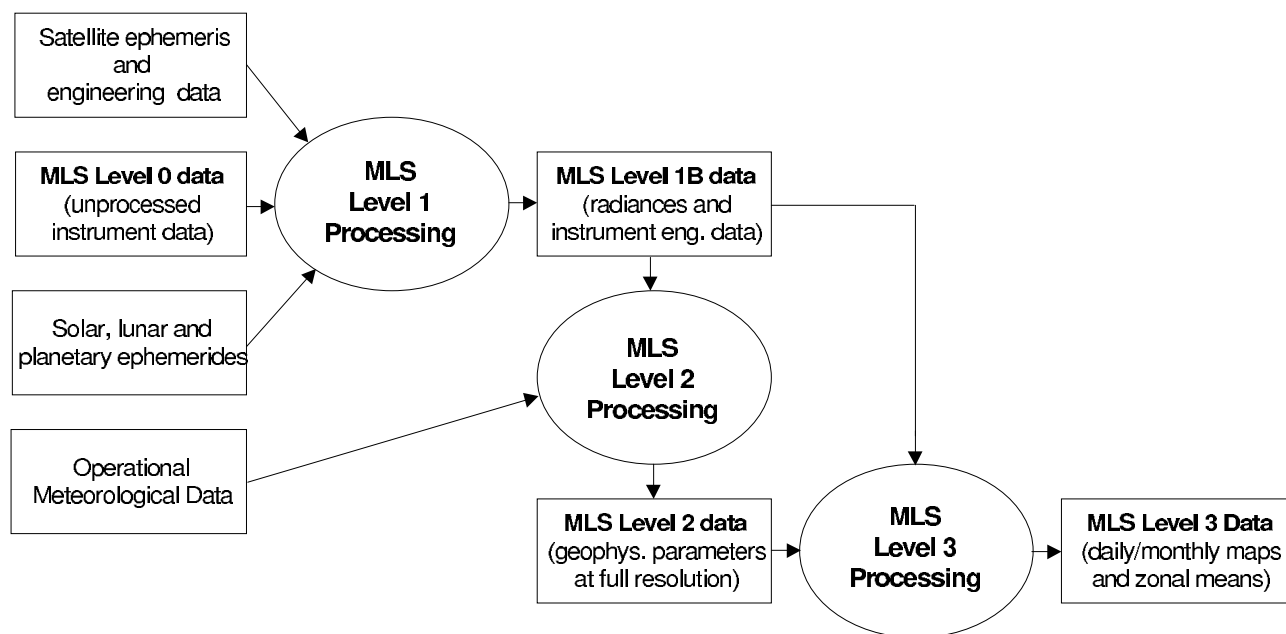The primary tasks of EOS MLS Level 1 data processing are to:

1. Qualify each datum using instrument configuration and checksum data, as well as transmission quality flags and statistical tests for 'reasonableness'.
2. Calibrate the instrument engineering data (e.g., voltages and temperatures).
3. Interpolate space (or other) 'reference' radiometric measurements to the time of calibration target and limb measurements.
4. Calculate radiometric gain at the time of the target measurements and interpolate it to the time of the limb measurements.
5. Estimate separately the spectrally-varying and spectrally-averaged component of the limb signal arising from antenna emission and scattering effects.
6. Calibrate the limb radiances and provide estimates of their uncertainties (for both the spectrally-varying and absolute values)
7. Determine the field-of-view boresight pointing angles for each radiometer.
8. Generate ancillary data (e.g., tangent point location, local solar time and zenith angles; flags for 'bright objects' in the field-of-view) which are needed for quality checks in Level 2 processing.
9. Produce daily files of the data and a log summarizing instrument performance and outputs.

The theoretical basis and algorithms for this processing are given by Jarnot (1999), and have heritage from UARS MLS.

The calibrated limb radiances produced by EOS MLS Level 1 processing are the values, for each spectral channel and instrument integration period, of the radiance received within approximately $6^o$ of the field-of-view boresight direction for that channel. (This is the angular range $\Omega_a$ over which the shape of the field-of-view is measured, as shown previously in Figure 5-7 for UARS MLS, and used in Level 2 processing. The small amount of radiance received outside $\Omega_a$ is estimated and removed during Level 1 processing.) The radiance is calibrated as average radiant power per unit spectral interval received by that channel; this measure of the received power has units of temperature which is convenient since the MLS signals originate thermally.

Briefly, the radiometric gain (counts per Kelvin) for channel $\alpha$ at the time of a target ($T$) observation is determined from the measured target and 'cold space' counts according to

$$g_\alpha(T) = \frac{C_\alpha^T - C_\alpha^S(T)}{aP^T - bP^S - c}$$

where $C_\alpha^T$ is the measured count for the target observation, $C_\alpha^S(T)$ is the 'cold space' count value interpolated to the time of the target measurement, $P^T$ is the measured target radiance (determined from its monitored temperature and measured emissivity), and $P^S$ is the measured 'cold space' radiance (that of a 2.7 K blackbody). Small effects due to baffles in the target and space views are accounted for by the near-unity factors $a$ and $b$, and - due to differences in 'baffle emission' between the two views - by the small term $c$. The preceding equation is equivalent to that of equation (4.17) of Jarnot (1999) which contains expressions for $a$, $b$ and $c$ in terms of quantities produced during instrument calibration.

The calibrated limb radiance power received by the antenna within angular range $\Omega_a$ for channel $\alpha$ is then produced according to

$$P_\alpha^A = \beta \left[ \frac{C_\alpha^L - C_\alpha^S(L)}{g_\alpha(L)} + \gamma P^S - \delta \right] - \varepsilon$$

where $C_\alpha^L$ is the measured count for the limb observation, $C_\alpha^S(L)$ is the 'cold space' count value interpolated to the time of the limb measurement, and $g_\alpha(L)$ is the radiometric gain interpolated to the time of the limb measurement. Small multiplicative effects (due, e.g., to antenna loss and scattering) are accounted for by the near-unity terms $\beta$ and $\gamma$, and small additive effects (due, e.g., to emission from the limb port baffle) are accounted for by the small terms $\delta$ and $\varepsilon$. The preceding equation is equivalent to that of equations (4.14) and (4.18) of Jarnot (1999) which contain expressions for $\beta$, $\gamma$, $\delta$ and $\varepsilon$ in terms of quantities produced during instrument calibration.

Calibration of limb radiances for the 'narrowband' digital autocorrelator spectrometer channels involves an additional Fourier transform step necessary to convert the measured autocorrelation function to spectral power density.

See Jarnot (1999) for development and details of the EOS MLS Level 1 data processing algorithms.

### 7.3 Level 2 data processing

The primary tasks of EOS MLS Level 2 data processing software are to:

1. Retrieve geophysical parameters such as temperature and composition from the EOS MLS Level 1B data, and provide estimates of the uncertainties on the retrieved quantities.

2. Produce additional diagnostic information (such as radiances calculated from the retrieved parameters, and chi-square statistics) on the quality of the retrieved geophysical parameters, and 'flags' to detect bad retrievals.

3. Produce ancillary data, such as tropopause pressure, which may be derived from MLS data and/or ancillary meteorological data available at the time of data processing.

4. Produce daily files of the output data, and a log summarizing appropriate information of the processing statistics for that day.

Livesey and Wu (1999) give the theoretical basis and algorithms for the MLS Level 2 data processing. The algorithms have heritage from UARS MLS, particularly the algorithms producing the most recent Version 5 UARS MLS data.

Retrieval theory, the basis of algorithms used to obtain geophysical parameters from remote measurements, is a well-established field in atmospheric science [Rodgers 1976 and 1990]. A 'state vector' $\mathbf{x}$ describes the atmospheric parameters being retrieved (as well as other quantities affecting the retrieval process), and a 'forward model' calculates estimates of the radiances (and other observables) from $\mathbf{x}$. The process is initialized by an assumed value of $\mathbf{x}$, and the retrieval algorithms, using the forward model, then adjust the elements of $\mathbf{x}$ to provide an optimal fit to the observed radiances. In addition to the radiance measurements, the retrieval algorithm uses 'virtual measurements' to improve the stability of the retrieval calculation, and the precision of the results. These virtual measurements are based on *a priori* knowledge of $\mathbf{x}$, often taken from climatological data sources. This *a priori* knowledge is also typically used to construct the starting value of $\mathbf{x}$.

The EOS MLS forward model is described by Read et al. (1999). Briefly, the forward model $f_\alpha(\mathbf{x})$ for the limb radiance power $P_\alpha^A$ received by the antenna within angular range $\Omega_a$ for channel $\alpha$ during an individual integration period is given by the integral radiative transfer equation integrated over the instrument response and FOV movement during the integration period $\Delta t$:

$$\overset{*}{P}_\alpha^A = \int_{\Delta t} \left[ \int_{\Omega_a} \int_\nu A_\alpha[\nu, \Omega, \Omega_0(t)] \left\{ I_\infty(\nu, \Omega)\, \tau(\nu, \infty) + \int_{s=\infty}^{s=0} \tau(\nu, s) \frac{dB[\nu, T(s)]}{ds} ds \right\} d\nu\, d\Omega \right] dt$$

$$\equiv\ f_\alpha(\mathbf{x})$$

where $\nu$ is frequency of the radiation, $\Omega$ is solid angle with $\Omega_o(t)$ being the FOV boresight direction at time $t$ and $\Omega_a$ the solid angle over which the FOV is measured during instrument calibration. $A_\alpha[\nu, \Omega, \Omega_o(t)]$ describes the instrument's spectral and FOV response for channel $\alpha$, and $I_\infty(\nu, \Omega)$ is the 2.7 K cosmic background emission. Distance along the ray path is $s$ (where the instrument is at $s = 0$), $T(s)$ is temperature and $B[\nu, T(s)]$ is the Planck blackbody function at $s$. The quantity $\tau(\nu, s)$ is the atmospheric transmission from $s$ to the instrument given by

$$\tau(\nu, s) = \exp\left[-\int_{s'=s}^{s'=0} k\left[\nu, T(s'), f(s'), \rho(s')\right] ds'\right],$$

where $k$ is the absorption coefficient as a function of frequency, temperature, mixing ratios $f$ of atmospheric species affecting the radiance, and atmospheric density $\rho$. The forward model equation, as written above, neglects scattering and assumes thermal equilibrium and that ray paths do not intersect the surface of the Earth. See Read et al. (1999) for development and details of the EOS MLS forward model.

The retrieval algorithms produce a value of the state vector $\mathbf{x}$ which is a best estimate of the true state of the atmosphere. The best estimate is defined as the value of $\mathbf{x}$ which most appropriately fits the measurements by minimizing the quantity $\chi^2$ for the difference between the measured and forward model radiances, properly accounting for correlations and inversely weighted by the noise covariance:

$$\chi^2 = \sum_i \left[\mathbf{y}_i - \mathbf{f}_i(\mathbf{x})\right]^T \mathbf{S}_i^{-1} \left[\mathbf{y}_i - \mathbf{f}_i(\mathbf{x})\right]$$

where $\mathbf{y}_i$ is a collection $i$ of the measured radiances $P_\alpha^A$, with noise covariance $\mathbf{S}_i$, and $\mathbf{f}_i(\mathbf{x})$ is the corresponding collection of radiances produced by the forward model. The superscript T indicates transpose.

The expression, which forms the basis for all MLS retrieval calculations, giving the recursive solution for the best estimate of the state vector $\mathbf{x}$ (typically starting from the *a priori* value $\mathbf{x}^{(0)} = \mathbf{a}$) is

$$\mathbf{x}^{(r+1)} = \mathbf{x}^{(r)} + \left[\mathbf{S}_\mathbf{a}^{-1} + \sum_i \mathbf{K}_i^T \mathbf{S}_i^{-1} \mathbf{K}_i\right]^{-1} \left\{\mathbf{S}_\mathbf{a}^{-1}\left[\mathbf{a} - \mathbf{x}^{(r)}\right] + \sum_i \mathbf{K}_i^T \mathbf{S}_i^{-1} \left[\mathbf{y}_i - \mathbf{f}_i(\mathbf{x}^{(r)})\right]\right\},$$

where

$$\mathbf{K}_i = \frac{\partial \mathbf{f}_i(\mathbf{x})}{\partial \mathbf{x}}$$

are known as the matrices of weighting functions for the measurements, and $\mathbf{S}_\mathbf{a}$ is the uncertainty covariance of $\mathbf{a}$. The uncertainty covariance for the retrieved state vector is given by

$$\mathbf{S}_\mathbf{x} = \left[\mathbf{S}_\mathbf{a}^{-1} + \sum_i \mathbf{K}_i^T \mathbf{S}_i^{-1} \mathbf{K}_i\right]^{-1}$$

Livesey and Read (1999) describe innovated extensions of the above expressions to direct retrieval of line-of-sight atmospheric structure as will be done on EOS MLS. See Livesey and Wu (1999) for development and details of the EOS MLS retrieval algorithms.

## 7.4 Level 3 data processing

The tasks of EOS MLS Level 3 data processing are to produce:

1. daily gridded maps of measurements which have adequate signal-to-noise for making such maps,

2. daily and monthly zonal means,

3. monthly gridded maps.

Fourier 'asynoptic mapping' techniques, as initially developed by Salby (1982), are planned to be used for producing the daily gridded maps. Jiang (1999) gives the theoretical basis for these techniques. They allow construction of a synoptic map from the MLS asynoptic measurements, and were applied to UARS MLS by Elson and Froidevaux (1993).

Optimum algorithms will be used for producing daily and monthly zonal means of 'noisy products', as described by Livesey and Wu (1999). Zonal means of products with adequate signal-to-noise for the daily gridded maps can be taken from the 'wavenumber zero' Fourier component generated during production of the daily maps.

Monthly gridded maps can be generated from the daily gridded maps by averaging the daily gridded data over a monthly period. Monthly gridded maps for 'noisy products' will be produced using the optimal algorithms described by Livesey and Wu (1999).

# 8. Data Products

## 8.1 Types of EOS MLS data products and examples of expected precisions

The following types of EOS MLS data products will be produced routinely.

Level 0 data

- 'Raw count' data from the instrument

Level 1 data

- Calibrated radiances with their estimated precisions for each MLS integration period and spectral channel, along with calibrated engineering data and merged ancillary data.

Level 2 data

- Geophysical products and their estimated precisions at full resolution along the measurement track, along with ancillary data such as time, location, local solar time, etc.,
- Diagnostics, such as geophysical parameters measured in more than one spectral band, tangent point pressure, chi-square statistics, etc.

Level 3 data

- Daily gridded maps of all geophysical data products, and their estimated precisions, that have sufficient precision for making such maps,
- Daily and monthly zonal means of all geophysical data products and their estimated precisions,
- Monthly global maps of all geophysical data products and their estimated precisions.

Table 8-1 gives estimates of the daily data volume for the MLS data products. The products are described in following subsections.

Table 8-1. The daily volume for EOS MLS routine data products. Values are in Megabytes.

| Level 0 | Level 1 | Level 2 | Level 3 | total |
|---------|---------|---------|---------|-------|
| ~1200 | ~4000 | ~80 | ~50 | ~5200 |

Tables 8-2, 8-3 and 8-4 give examples and expected precisions of some MLS geophysical data products. The precisions given in these tables are from numerical calculations by M. J. Filipiak based on the expected MLS instrument noise (given in Table 5-2) and the planned limb scan profiles (given in Figure 6-2). See Filipiak (1999) for a description of these calculations, and plots of sensitivity versus height for all the MLS geophysical data products.

Absolute 'stand-alone' (i.e., without use of correlative data) accuracy of most products, based on experience from UARS MLS, is expected to be typically ~5% for composition measurements and ~1-2 K for temperature.

Table 8-2. Expected precision (1σ) for some MLS Level 2 profiles produced every 165 km along the measurement track, and for MLS Level 3 daily maps with ~5° latitude resolution. (From Filipiak 1999). The estimated precisions for cloud ice, and their effect on $H_2O$, CO and $O_3$ measurements, assume the cloud ice particles are smaller than ~100 μm so that scattering of the MLS signals can be neglected. 'Moderate cirrus' mentioned in the table are assumed to have 0.05 $g/m^3$ ice content, and 'thick cirrus' to have 0.5 $g/m^3$. 'ppbv' indicates $10^{-9}$ volume mixing ratio.

| Geophysical Parameter (alphabetical order) | Expected vertical range for useful measurements | Expected precision at indicated heights (for ~3 km vertical resolution, unless otherwise indicated) | |
|---|---|---|---|
| | | Level 2 profiles (produced every 165 km along track) | Level 3 daily maps (for ~5° latitude resolution) |
| cirrus ice | ~10-20 km | ~0.001 $gm/m^3$ avg over MLS FOV within ~5 km of tropical tropopause ~0.005 $gm/m^3$ avg over MLS FOV within ~2 km of high latitude tropopause | |
| ClO | ~15-40 km | ~0.4 ppbv @ 35 km ~0.2 ppbv @ 20 km ~0.3 ppbv @ 15 km | ~0.3 ppbv @ 35 km ~0.1 ppbv @ 20 km ~0.2 ppbv @ 15 km |
| CO | ~10-15 km | ~50 ppbv @ 15 km ~60 ppbv @ 10 km in tropics | ~30 ppbv @ 15 km ~40 ppbv @ 10 km in tropics |
| | | The presence of thin cirrus will not degrade the preceding precisions, which assume clear sky. Moderate cirrus are expected to increase the 10 km tropical values ~1.1×. Thick cirrus are expected to increase the 10 km tropical values ~3×. | |
| geopotential height | ~5-80 km | ~15 m @ 5-30 km ~30 m @ 40 km ~70 m @ 50 km | ~10 m @ 5-30 km ~20 m @ 40 km ~40 m @ 50 km |
| $H_2O$ | ~5-80 km | ~20% @ 50 km ~10% @ 35 km ~5% @ tropopause ~20% @ trop for 2 km vert res. ~5% @ 5 km ~50% @ 5-10 km for 1 km vert. resolution | ~10% @ 50 km ~5% @ 35 km ~3% @ tropopause ~10% @ trop for 2 km vert. res. ~3% @ 5 km ~30% @ 5-10 km for 1 km vert. resolution. |
| | | The presence of thin cirrus will not degrade the preceding precisions, which assume clear sky. Moderate cirrus increase them ~1.2-1.5× in the tropics and ~1.5-3× at high latitudes. Thick cirrus increase them ~2-3× in the tropics, ~2-6× at high latitudes, depending upon altitude. | |
| HCl | ~15-60 km | ~1 ppbv @ 50 km ~0.2 ppbv @ 25 km ~0.3 ppbv @ 15 km | ~0.7 ppbv @ 50 km ~0.1 ppbv @ 25 km ~0.2 ppbv @ 15 km |
| HCN | ~10-30 km | ~0.15 ppbv @ 30 km (5 km resolution) ~0.07 ppbv @ 20 km (5 km resolution) ~0.15 ppbv @ 10 km (5 km resolution) | ~0.09 ppbv @ 30 km (5 km resolution) ~0.04 ppbv @ 20 km (5 km resolution) ~0.1 ppbv @ 10 km (5 km resolution) |
| $HNO_3$ | ~15-30 km | ~4 ppbv @ 25 km ~3 ppbv @ 20 km ~3 ppbv @ 15 km | ~3 ppbv @ 25 km ~2 ppbv @ 20 km ~2 ppbv @ 15 km |
| $N_2O$ | ~10-40 km | ~40 ppbv @ 40 km ~20 ppbv @ 25 km ~50 ppbv @ 15 km | ~30 ppbv @ 40 km ~15 ppbv @ 25 km ~30 ppbv @ 15 km |
| $O_3$ | ~10-80 km | ~10% @ 50 km ~2% @ 30 km ~10% @ 3 km above tropopause ~10 ppbv @ 3 km below tropopause in tropics | ~5% @ 50 km ~1% @ 30 km ~5% @ 3 km above tropopause ~7 ppbv @ 3 km below tropopause in tropics |
| | | The presence of thin cirrus will not degrade the preceding precisions, which assume clear sky. Moderate cirrus are expected to increase the '3 km below tropopause' tropical values ~1.5×. Thick cirrus are expected to increase the '3 km below tropopause' tropical values ~3.5×. | |
| OH | ~35-60 km | ~0.15 ppbv @ 50 km ~0.008 ppbv @ 30 km | ~0.1 ppbv @ 50 km ~0.005 ppbv @ 30 km |
| $SO_2$ | ~15-35 km | ~3 ppbv @ 35 km ~1 ppbv @ 15-25 km | ~2 ppbv @ 35 km ~0.7 ppbv @ 20 km |
| temperature | ~5-80 km | ~2 K @ 40 km ~0.5 K @ 10-30 km ~1 K @ 5 km | ~1.5 K @ 40 km ~0.3 K @ 10-30 km ~0.6 K @ 5 km |

Table 8-3. Expected precision (1σ) for some MLS Level 3 daily and monthly zonal means (from Filipiak 1999). The precisions here assume clear sky conditions in the troposphere. Degradations in expected precision for $H_2O$, CO and $O_3$ due to the presence of cirrus are given in the Table 8-2 entries for these measurements. 'ppbv' indicates $10^{-9}$ volume mixing ratio, and 'pptv' indicates $10^{-12}$ volume mixing ratio.

| Geophysical Parameter | ~ range for useful data | Expected precision at indicated heights (for ~3 km vertical and 5° latitude resolution unless otherwise stated) | |
| --- | --- | --- | --- |
| | | daily 5° zonal mean | monthly 5° zonal mean |
| BrO | ~20-40 km | not expected to be useful | ~5 pptv (~20%) @ 35 km, for 5 km res<br>~3 pptv (~30%) @ 20 km, for 5 km res |
| ClO | ~15-60 km | ~0.1 ppbv (~20%) @ 40 km<br>~0.04 ppbv (~10%) @ 30 km<br>~0.02 ppbv @ 20 km<br>~0.04 ppbv @ 15 km | ~0.02 ppbv (~5%) @ 40 km<br>~0.008 ppbv (~2%) @ 30 km<br>~0.004 ppbv (~5%) @ 20 km<br>~0.007 ppbv @ 15 km |
| CO | ~8-60 km | ~10 ppbv (~30-50%) @ 30 km<br>~5 ppbv (~20%) @ 20 km<br>~7 ppbv (~10%) @ 10 km | ~10% @ 20-50 km<br>~10% @ high latitude winter tropopause<br>~3% @ tropical tropopause<br>~3% @ 3 km below tropical tropopause<br>~30% @ 3 km below high lat winter tropopause |
| HCl | ~12-60 km | ~0.1 ppbv (3%) @ 50 km<br>~0.02 ppbv (~2%) @ 25 km<br>~0.03 ppbv (~10-30%) @ 15 km | ~0.02 ppbv (~1%) @ 50 km<br>~0.004 ppbv (~0.5%) @ 25 km<br>~0.006 ppbv (~2-5%) @ 15 km |
| HCN | ~8-50 km | ~30 pptv @ 40 km<br>~10 pptv (~5-10%) @ 15-25 km<br>~20 pptv (~10%) @ 10 km | ~5 pptv @ 40 km<br>~3 pptv (~1-2%) @ 15-25 km<br>~5 pptv (~2%) @ 10 km |
| HOCl | ~25-45 km | will probably not be useful | ~0.02 ppbv (~20% at low-mid lat) @30 km |
| HO₂ | ~25-60 km | not expected to be useful | ~100 pptv (~30% at low latitudes) @ 50 km<br>~30 pptv (~20% at low latitudes ) @ 40 km<br>~10 pptv (~25% at low latitudes ) @ 30 km |
| OH | ~20-60 km | ~20 pptv (~5%) @ 50 km<br>~5 pptv (~10%) @ 40 km<br>~1 pptv (~30%) @ 30 km<br>not expected to be useful below ~30 km | ~4 pptv (~1%) @ 50 km<br>~1 pptv (~1%) @40 km<br>~0.2 pptv (~3%) @ 30 km<br>~0.4 pptv (~50%) @ 20 km |
| H₂O | ~5-80 km | ~2% @ 50 km for 3 km resolution<br>~1% or better @ 5-30 km for 3 km resolution<br>~5-30% @ 5 km to trop for 1 km resolution | in principle, should be ~5x better than daily zonal means, but not yet clear how much of this improvement can be achieved due to various effects which become important at such small percentage levels |
| O₃ | ~10-80 km | <1% for ~18-45 km<br>~3% at tropopause<br>~2% (~1 ppbv) at 3 km below trop in tropics | |
| temperature | ~5-80 km | ~0.5 K @ 50 km<br>~0.2 K @ 35 km<br>~0.1 K @ tropopause to 30 km<br>~0.2 K @ 5 km | |

Table 8-4. Expected precision (1σ) for some MLS Level 3 monthly maps (from Filipiak 1999). The precisions here assume clear sky conditions in the troposphere. Degradations in expected precision for $H_2O$, CO and $O_3$ due to the presence of cirrus are given in the Table 8-2 entries for these measurements.

| Geophysical Parameter | Expected vertical range for useful meas | Expected precision at indicated heights (for ~3 km vertical resolution and ~5o latitude resolution, unless otherwise indicated) |
| --- | --- | --- |
| CO | ~8-30 km | ~10 ppbv (~30-50%) @ 30 km<br>~5 ppbv (~10%) @ tropical tropopause<br>~10 ppbv (~15%) @ polar winter tropopause<br>~7 ppbv (~10%) @ 10 km in tropics |
| H₂O | ~5-80 km | ~3% @ 50 km<br>~1% @ 30 km<br>~0.5% @ 20 km<br>~0.5% @ tropopause<br>~0.3-1% @ 3 km below trop<br>~1% @ 5 km |
| O₃ | ~8-80 km | ~0.3-1% @ 18-45 km<br>~2-5 ppbv (~2-10%) @ tropopause<br>~2 ppbv (~5%) @ 3 km below trop in tropics<br>~10 ppbv (~20%) @ 3 km below trop in polar winter |

## 8.2  Level 0 data products

MLS Level 0 products are reconstructed unprocessed instrument data at full resolution with any and all communications artifacts removed.  Table 8-5 lists the general contents, and daily volume.

Table 8-5.  MLS Level 0 data

|  | daily volume / Megabytes |
|---|---|
| unprocessed spectrometer and filter data (science data) | 1100 |
| unprocessed instrument engineering data | ~3 |
| ancillary data (e.g., various spacecraft engineering data merged into MLS instrument data stream in orbit) | ~1 |
| **total (including contingency)** | **~1200** |

## 8.2  Level 1 data products

MLS Level 1 data products are calibrated instrument data at full resolution, calibrated instrument engineering data, performance diagnostics, and ancillary data.  These are classified as Level 1B data in EOS terminology (p. 40 of MTPE EOS Reference Handbook 1995).  There will be no Level 1A data product ('unprocessed instrument data ... with ... radiometric and geometric calibration coefficients and georeferencing parameters ... computed and appended'); such a data product is neither needed nor appropriate for MLS because all the 'Level 1A' information is either in the MLS Level 0 or Level 1B data.

Table 8-6 lists the general contents and daily volume of MLS Level 1 data. There is one data file per day, each file corresponding to 00-24 hours Greenwich Mean Time (GMT).

Table 8-6. MLS Level 1B data

|  | daily volume / Megabytes |
|---|---|
| calibrated limb radiances and estimated precisions | 2700 |
| processed instrument engineering data | 7 |
| diagnostics (e.g., radiometric gains, chi-square statistics) | 700 |
| ancillary data | tbd, small |
| **total (including contingency)** | **~4000** |

The ancillary data include items such as:

time

spacecraft altitude, location and velocity

spacecraft attitude and attitude rate of change

spacecraft inertial reference unit (IRU) and gyroscope status

spacecraft IRU gyroscope angle

various spacecraft voltages, temperatures and other engineering data

flags (or angles) indicating potential 'bright object' (e.g., moon) interference in GHz or THz FOV

location (latitude, longitude, height) of nominal GHz and THz FOV tangent points

local solar time and solar zenith angle at nominal GHz and THz FOV tangent points

angle between north and the MLS line of sight at the tangent point

See Jarnot (1999) for a detailed description on the MLS Level 1B ancillary data.

## 8.3  Level 2 data products

There is one data file per day for each of the Level 2 data products.  Each file corresponds to 00-24 hours GMT.

Present plans are to produce Level 2 geophysical parameters on a vertical grid having 12 points per decade change in pressure, and on a horizontal grid having points near the nominal tangent point locations of each limb scan (every 1.5° great circle along the measurement track), as shown earlier in Figures 6-2 and 6-3.  The vertical grid density  (adjacent points are separated between ~1 and ~1.5 km in height, depending upon atmospheric temperature) was chosen in order to be capable of representing the best vertical resolution expected from EOS MLS and, at the same time, to be a superset of the vertical grid used for UARS Level 3 data.  Figure 8-1 shows vertical spacing between adjacent pressure surfaces for 3, 6 and 12 points per decade pressure, and the vertical extent of the EOS MLS fields-of-view (FOV).  The vertical extent of the 63 GHz UARS MLS FOV is also shown for comparison.  Good temperature profiles were obtained from the UARS MLS 63 GHz measurements at a resolution of 3 points per decade pressure (about half the field-of-view width), which demonstrated the capability to obtain vertical resolution better than that indicated solely by the MLS FOV width.  Vertical smoothing will be done by the retrieval algorithms, or by averaging profile points, as needed to give a stable product and reduce noise.
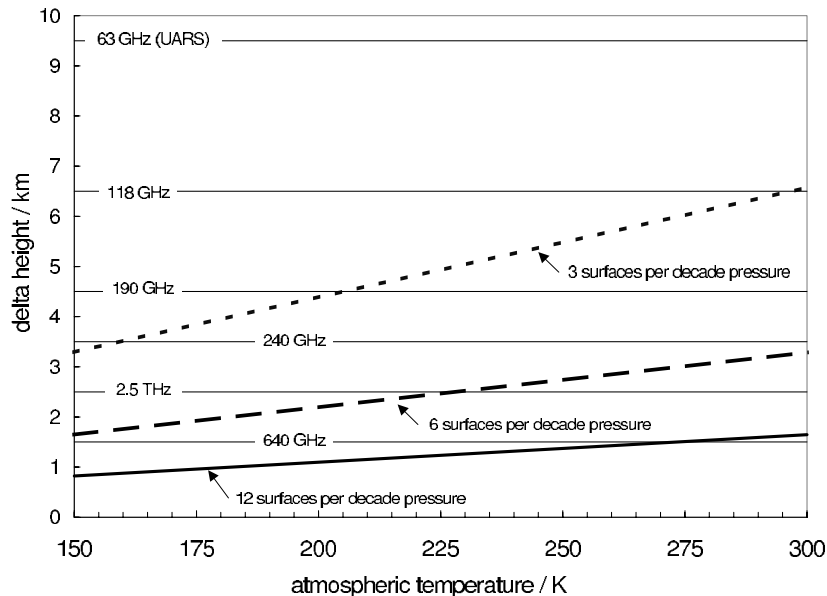


Figure 8-1.  Height between atmospheric pressure surfaces (sloping lines) for different numbers of surfaces per decade pressure, and vertical extent of the fields-of-view (horizontal lines) at the limb tangent point for the various EOS MLS radiometers.  The vertical extent of the field-of-view for the UARS MLS 63 GHz radiometer is also shown.

Table 8-7 shows ancillary data that will be included with each MLS Level 2 retrieved profile (one set of values per profile).  The data quality flag will likely, as was the case for UARS MLS, be based on chi-square statistics indicating the quality of fit to the measured radiances and other diagnostics such as the number of radiances that were used in the retrieval of that profile.

Table 8-7.  Ancillary data included with each MLS Level 2 vertical profile.

| name | units | comments |
|---|---|---|
| time | TBD | ~ 1 second resolution |
| latitude | degrees N | ~0.1 degree resolution |
| longitude | degrees E | ~0.1 degree resolution |
| local solar time | hours | ~0.01 hour resolution |
| local solar zenith angle | degrees | ~0.1 degree resolution |
| tangent point line-of-sight angle *wrt* north | degrees E | ~1 degree resolution |
| data quality flag | none | indicates overall profile quality |

## 8.3.1 Level 2 Geophysical Data Products

Table 8-8 lists the standard Level 2 geophysical data products from EOS MLS.

The vertical range for each product given in Table 8-8 extends slightly beyond the limits where MLS is expected to produce useful information and values at the limits will relax to climatology or operational meteorological data. (Note: the range given here may not extend sufficiently high for temperature, $O_3$, $N_2O$ and CO, and this may be revised when simulation studies are more mature.)

Table 8-8. Level 2 standard geophysical data products for EOS MLS. 'vmr' indicates 'volume mixing ratio' and 'DU' indicates 'Dobson Unit'. These products are consistent with the MLS standard data products stated for MLS in the EOS CHEMISTRY Project Plan (NASA Goddard Space Flight Document 424-PG-7120.2.1) dated 15 April 1999. Data volumes given here assume 12 retrieval points per decade pressure for each product (the maximum planned for each and these estimates are thus conservative), and a 4-byte word each for the value and estimated precision. The volume estimates include ancillary data given earlier in Table 8-7.

| data product (alphabetical order) | units | nominal vertical range | | | | nominal number of pressure surfaces | nominal volume for one day / Megabytes |
| --- | --- | --- | --- | --- | --- | --- | --- |
| | | pressure / hPa | | ~ height / km | | | |
| | | max | min | min | max | | |
| BrO | vmr | 100 | 1 | 15 | 50 | 24 | 0.75 |
| cirrus ice average density | avg gm/m$^3$ | 464 | 46 | 5 | 20 | 12 | 0.41 |
| ClO mixing ratio | vmr | 100 | 0.1 | 15 | 65 | 36 | 1.08 |
| CO mixing ratio | vmr | 464 | 0.001 | 5 | 95 | 68 | 1.98 |
| geopotential height | km | 1000 | 0.01 | 0 | 80 | 60 | 1.76 |
| $H_2O$ mixing ratio | vmr | 1000 | 0.001 | 0 | 95 | 72 | 2.10 |
| HCl mixing ratio | vmr | 464 | 0.01 | 5 | 80 | 56 | 1.65 |
| HCN mixing ratio | vmr | 464 | 1 | 5 | 50 | 32 | 0.97 |
| $HNO_3$ mixing ratio | vmr | 464 | 1 | 5 | 50 | 32 | 0.97 |
| $HO_2$ mixing ratio | vmr | 100 | 0.1 | 15 | 65 | 36 | 1.08 |
| HOCl mixing ratio | vmr | 100 | 1 | 15 | 50 | 24 | 0.75 |
| $N_2O$ mixing ratio | vmr | 464 | 1 | 5 | 50 | 32 | 0.97 |
| $O_3$ mixing ratio | vmr | 464 | 0.001 | 5 | 95 | 68 | 1.98 |
| $O_3$ stratospheric column | DU | not applicable | | | | | 0.10 |
| OH mixing ratio | vmr | 100 | 0.01 | 15 | 80 | 48 | 1.42 |
| relative humidity | % wrt ice | 1000 | 46 | 0 | 15 | 12 | 0.41 |
| $SO_2$ mixing ratio | vmr | 100 | 3.2 | 15 | 40 | 18 | 0.58 |
| temperature | K | 1000 | 0.001 | 0 | 95 | 72 | 2.10 |
| total geophysical data product volume for 1 day | | | | | | | 21.0 |

## 8.3.2 Level 2 Diagnostic Products

The EOS MLS Level 2 diagnostic products, listed in Table 8-9, fall into three categories:

(a) geophysical parameters obtained from an individual spectral band, when the same parameter is measured by more than one spectral band. This provides information for eliminating systematic problems in the overall measurement system.

(b) certain additional geophysical quantities that are needed for diagnostic purposes, such as cloud extinction coefficients derived from various MLS bands and tropopause pressure derived from a combination of MLS and operational meteorological data.

(c) diagnostics (e.g., retrieved tangent pressure, chi-square statistics, retrieved instrument artifacts such as spectral baseline) needed for monitoring the Level 2 algorithm performance.

Table 8-9. Nominal Level 2 diagnostic products. Volumes here assume 12 points per decade pressure for geophysical quantities, 4-byte words for the value and uncertainty, and ancillary data in Table 8-7.

| diagnostic product | units | vertical range pressure / hPa max | min | ~ height /km min | max | number of pressure surfaces | volume for one day / Mbyte |
|---|---|---|---|---|---|---|---|
| temperature from 118 GHz 'a' (primary) radiometer | K | 1000 | 0.001 | 0 | 95 | 72 | 2.10 |
| temperature from 118 GHz 'b' (redundant) radiometer | K | 1000 | 0.001 | 0 | 95 | 72 | 2.10 |
| temperature from 240 GHz radiometer | K | 1000 | 1 | 0 | 50 | 36 | 1.08 |
| tropospheric $H_2O$ from 118 GHz radiometer | vmr | 1000 | 46 | 0 | 20 | 16 | 0.52 |
| tropospheric $H_2O$ from 190 GHz radiometer | vmr | 1000 | 46 | 0 | 20 | 16 | 0.52 |
| tropospheric $H_2O$ from 240 GHz radiometer | vmr | 1000 | 46 | 0 | 20 | 16 | 0.52 |
| tropospheric $H_2O$ from 640 GHz radiometer | vmr | 1000 | 46 | 0 | 20 | 16 | 0.52 |
| tropospheric $H_2O$ from 2.5 THz radiometer | vmr | 1000 | 46 | 0 | 20 | 16 | 0.52 |
| relative humidity from 118 GHz radiometer | % wrt ice | 1000 | 46 | 0 | 20 | 16 | 0.52 |
| relative humidity from 190 GHz radiometer | % wrt ice | 1000 | 46 | 0 | 20 | 16 | 0.52 |
| relative humidity from 240 GHz radiometer | % wrt ice | 1000 | 46 | 0 | 20 | 16 | 0.52 |
| relative humidity from 640 GHz radiometer | % wrt ice | 1000 | 46 | 0 | 20 | 16 | 0.52 |
| relative humidity from 2.5 THz radiometer | % wrt ice | 1000 | 46 | 0 | 20 | 16 | 0.52 |
| $O_3$ from 190 GHz radiometer | vmr | 100 | 0.1 | 15 | 65 | 36 | 1.08 |
| $O_3$ from 240 GHz radiometer 3.9 GHz IF band | vmr | 464 | 0.001 | 5 | 95 | 68 | 1.98 |
| $O_3$ from 240 GHz radiometer 9.1 GHz IF band | vmr | 464 | 1 | 5 | 50 | 32 | 0.97 |
| $O_3$ from 640 GHz radiometer | vmr | 464 | 0.1 | 5 | 65 | 44 | 1.31 |
| ClO from 190 GHz radiometer | vmr | 100 | 0.1 | 15 | 65 | 36 | 1.08 |
| ClO from 640 GHz radiometer | vmr | 100 | 0.1 | 15 | 65 | 36 | 1.08 |
| $N_2O$ from 190 GHz radiometer | vmr | 464 | 1 | 5 | 50 | 32 | 0.97 |
| $N_2O$ from 640 GHz radiometer | vmr | 464 | 1 | 95 | 50 | 32 | 0.97 |
| OH from 2.514 THz spectral line, horizontal polarization | vmr | 100 | 0.01 | 15 | 80 | 48 | 1.42 |
| OH from 2.514 THz spectral line, vertical polarization | vmr | 100 | 0.01 | 15 | 80 | 48 | 1.42 |
| OH from 2.510 THz spectral line, horizontal polarization | vmr | 100 | 0.01 | 15 | 80 | 48 | 1.42 |
| OH from 2.510 THz spectral line, vertical polarization | vmr | 100 | 0.01 | 15 | 80 | 48 | 1.42 |
| $HO_2$ from 649.7 GHz spectral line | vmr | 100 | 0.1 | 15 | 65 | 36 | 1.08 |
| $HO_2$ from 660.5 GHz spectral line | vmr | 100 | 0.1 | 15 | 65 | 36 | 1.08 |
| BrO from 624.8 GHz spectral line | vmr | 100 | 1 | 15 | 50 | 24 | 0.75 |
| BrO from 650.2 GHz spectral line | vmr | 100 | 1 | 15 | 50 | 24 | 0.75 |
| $SO_2$ from 190 GHz radiometer | vmr | 100 | 3.2 | 15 | 40 | 18 | 0.58 |
| $SO_2$ from 640 GHz radiometer | vmr | 100 | 3.2 | 15 | 40 | 18 | 0.58 |
| 'cloud' extinction parameters (20 values assumed for now) | $km^{-1}$ | 1000 | 46 | 0 | 20 | 16 | 10.42 |
| parameters related to tropopause pressure (see note below) | hPa | not applicable | | | | | 0.21 |
| subtotal, geophysical diagnostic quantities total daily data volume | | | | | | | 41.08 |
| miscellaneous additional diagnostics (tangent pressure, chi-square statistics, retrieved instrument artifacts, etc.) | | | | | | | ~20 |
| estimated total daily data volume | | | | | | | ~60 |

Note: 'parameters related to tropopause pressure' is now planned to contain:
(a) pressure at tropopause defined by operational temperature data sets available at time of MLS data processing
(b) pressure at the tropopause as defined by the MLS temperature profile
(c) lowest pressure at which MLS detects water vapor abundances characteristic of troposphere (needs more definition)
(d) perhaps other related quantities (space is budgeted for two additional quantities in table above)

The EOS MLS Level 2 software will also be capable of outputting the radiances calculated for the retrieved state vector, in order to diagnose residual differences from the observed radiances. This will be done, mainly, during initial testing of the algorithms and for individual case studies, but (primarily because of the large data volumes involved) will probably not be done routinely.

## 8.4 Level 3 data products

### 8.4.1 Level 3 Daily Map Products

Daily gridded map products will be made for MLS measurements which have adequate signal-to-noise. Fourier techniques, as initially developed by Salby (1982) will likely be used to produce 'synoptic' maps of the data. The current plan is for a map output grid of $4^o$ longitude by $2^o$ latitude (between 82 N and 82 S), and with the daily maps produced for a time corresponding to noon GMT. Table 8-10 gives the currently-planned daily map products. Separate maps for data from the ascending and descending portions of the orbit will be made for the diurnally-varying species ClO, OH, and $O_3$ at higher altitude. The value and estimated precision are included in the data files. The Level 3 daily map files will also include coefficients (e.g., coefficients of the Fourier wavenumbers and frequencies) generated as intermediate products in production of the maps The software that produces these maps shall be capable of producing similar maps from any MLS Level 2 geophysical data file, including files for the diagnostic geophysical data products.

Table 8-10. Nominal Level 3 Daily Map Products. The number of pressure surfaces and volumes assume 12 retrieval points per decade pressure (the maximum value planned), and 4-byte words for the value and precision at each grid point. The volumes account for storage of the map coefficients (assumed to have increased the volume by 50%).

| name (alphabetical order) | units | vertical range | | | | number of pressure surfaces | volume for one day / Megabytes |
|---|---|---|---|---|---|---|---|
| | | pressure/hPa | | ~ height / km | | | |
| | | max | min | min | max | | |
| ClO mixing ratio from ascending part of orbit | vmr | 100 | 1 | 15 | 50 | 24 | 2.15 |
| ClO mixing ratio from descending part of orbit | vmr | 100 | 1 | 15 | 50 | 24 | 2.15 |
| geopotential height | km | 464 | 0.01 | 0 | 80 | 56 | 5.03 |
| $H_2O$ mixing ratio | vmr | 464 | 0.01 | 0 | 80 | 56 | 5.03 |
| HCl mixing ratio | vmr | 100 | 0.1 | 15 | 65 | 36 | 3.23 |
| HCN mixing ratio | vmr | 215 | 22 | 9 | 25 | 12 | 1.08 |
| $HNO_3$ mixing ratio | vmr | 100 | 1 | 15 | 50 | 24 | 2.15 |
| $N_2O$ mixing ratio | vmr | 215 | 1 | 9 | 50 | 28 | 2.51 |
| $O_3$ mixing ratio | vmr | 316 | 0.32 | 9 | 80 | 36 | 3.23 |
| $O_3$ mixing ratio from ascending part of orbit | vmr | 3.16 | 0.01 | 40 | 80 | 30 | 2.69 |
| $O_3$ mixing ratio from descending part of orbit | vmr | 3.16 | 0.01 | 40 | 80 | 30 | 2.69 |
| $O_3$ stratospheric column | DU | not applicable | | | | | 0.09 |
| OH mixing ratio from ascending part of orbit | vmr | 10 | 0.1 | 15 | 65 | 24 | 2.15 |
| OH mixing ratio from descending part of orbit | vmr | 10 | 0.1 | 15 | 65 | 24 | 2.15 |
| temperature | K | 464 | 0.01 | 0 | 80 | 56 | 5.03 |
| estimated total daily volume | | | | | | | 41.33 |

### 8.4.2 Level 3 Daily Zonal Mean Products

Daily zonal mean products will be produced for all the MLS Level 2 products. MLS Level 3 daily zonal mean geophysical products correspond to the Level 2 geophysical products, and Level 3 daily zonal mean diagnostic products correspond to the Level 2 diagnostic geophysical products. Current plans are to produce separate zonal means for the ascending (mostly day) and descending (mostly night) portions, and the full latitudinal resolution of the corresponding Level 2 product is maintained (i.e., a zonal mean is produced for each of the Level 2 latitudes), which gives better latitude resolution at high latitudes. The value and estimated precision in the daily zonal mean are included in the data files. Ancillary data included with the geophysical parameters are latitude, local solar time and local solar zenith angle. Table 8-11 gives the daily data volumes for these products. The value and estimated precision are included in the data files.

Table 8-11. Data volumes for Level 3 daily zonal mean products

|  | daily volume / Megabytes |
|---|---|
| geophysical products | 1.43 |
| diagnostic products | 2.28 |

### 8.4.3 Level 3 Monthly Map Products

Level 3 monthly map products will be produced for all MLS Level 2 products. MLS Level 3 monthly geophysical map products correspond to Level 2 geophysical products, and monthly diagnostic map products correspond to the Level 2 diagnostic geophysical products. These maps represent average conditions for the month and are currently planned to be produced at the $2^o$ latitude by $4^o$ longitude grid used for the Level 3 daily maps. Separate maps for the ascending and descending sides of the orbit will be produced for diurnally-varying species (ClO, OH, $HO_2$, BrO and HOCl). The 'month' for these maps is defined to be the same as calendar months but, perhaps, with 'February' including 31 January and 1 March to give either 30 or 31 days for each 'EOS MLS month'. Equivalent daily data volumes are given in Table 8-12. The value and estimated precision are included in the data files.

Table 8-12. Data volumes for Level 3 monthly map products. The equivalent daily volume is the monthly volume divided by 30.

|  | equivalent daily volume / Megabytes |
|---|---|
| geophysical products | 0.87 |
| diagnostic products | 1.11 |

### 8.4.4 Level 3 Monthly Zonal Mean Products

Level 3 monthly zonal mean products will be produced for all the MLS Level 2 products. MLS Level 3 monthly geophysical zonal mean products correspond to the Level 2 geophysical products, and Level 3 monthly diagnostic zonal mean products correspond to the Level 2 diagnostic geophysical products. Current plans are to produce separate zonal means for the ascending (mostly day) and descending (mostly night) portions of the orbit, and the full latitudinal resolution of the

corresponding Level 2 product is maintained (i.e., a zonal mean is produced for each of the Level 2 latitudes), which gives better latitude resolution at high latitudes. The value and estimated precision in the monthly zonal mean are included in the data files. Ancillary data included with the geophysical parameters are latitude, and maximum and minimum values of the local solar time and local solar zenith angle for the measurement over the course of the month. Table 8-13 gives the equivalent daily data volumes for these products.

Table 8-13. Data volumes for Level 3 monthly zonal mean products. The equivalent daily volume is the monthly volume divided by 30.

|  | equivalent daily volume / Megabytes |
|---|---|
| geophysical products | 0.05 |
| diagnostic products | 0.08 |

# 9. Data Validation

Validation of the EOS MLS data products will follow the same procedures used successfully for UARS MLS data, and documented in the UARS MLS data validation publications (see references cited in section 2 of this document). These include the following:

1. Simulation and sensitivity studies to determine the expected precision and absolute accuracy of each data product.

2. Inspection of all incoming data, and certain diagnostics, for 'reasonableness' and unexpected 'spikes' through examination of a manageable number of routine analyses products.

3. Examination of radiance residuals as a function of observation tangent pressure and signal frequency to determine, and hopefully eliminate, artifacts.

4. Comparison of the same geophysical parameter measured in more than one spectral region.

5. Comparison of MLS measurements with measurements of the same geophysical parameters by other instruments on the EOS CHEM mission.

6. Comparison with other 'correlative measurements' from aircraft, balloon, and ground-based measurements.

A scientist on the MLS team who is knowledgeable in its scientific use will be responsible for the validation of each geophysical data product. Table 1-1, in section 1 of this document, gives current responsibilities.

Table 9-1 gives correlative measurement priorities for EOS MLS.

The following data will also be very valuable for improving the quality of the EOS MLS measurements:

1. Better laboratory measurements and theoretical expressions for water vapor and dry air continuum absorption at frequencies between 100 and 2500 GHz, and for conditions representative of the upper troposphere. These will improve the absolute accuracy of the MLS upper tropospheric $H_2O$ measurement.

2. More measurements, and development of a 'climatology', of cirrus particle concentration and size distribution, especially for particles larger than ~100 μm. These would improve interpretation of the MLS cirrus ice measurement.

3. Better laboratory measurements of linewidth parameters for certain spectral lines (specific lines to be documented later).

Details of MLS data validation are in the EOS MLS Data Validation Plan (Froidevaux, et al. 1999).

Table 9-1. EOS MLS correlative measurement priorities. Correlative measurements for the upper troposphere and lower stratosphere are considered most valuable because these regions are being emphasized by the CHEM mission. Measurements are in approximate decreasing order of priority within each row of the 'parameter' column. However, the lower priority measurements in one row are not necessarily higher in priority than the higher priority measurements in another row.

| category | parameter | comments |
|---|---|---|
| most valuable | upper tropospheric $O_3$, CO, $H_2O$, HCN and temperature | Aircraft measurements of the vertical profile along the MLS track are especially valuable, particularly in the tropical tropopause regions. Tropical sonde data for $O_3$ and $H_2O$ are also especially valuable. |
| | lower stratospheric OH, $HO_2$, BrO, $O_3$, $H_2O$, ClO, HCl, HOCl, $N_2O$, $HNO_3$, temperature, geopotential height, HCN, CO and $SO_2$ | Aircraft measurements along the MLS track and balloon measurements of the vertical profile are needed. |
| | Upper tropospheric cloud data: number density and size distribution of particles larger than ~100 μm, total ice and liquid density | In particular, measurements for clouds above ~8 km in the tropics (along the MLS measurement track if possible). |
| very valuable | middle and upper stratospheric OH, $HO_2$, BrO, HOCl, $O_3$, HCl, ClO, $H_2O$, $HNO_3$, HCN, CO, temperature, geopotential height | Measurements of the vertical profile are needed |

# References

Asrar, G., and J. Dozier, *EOS Science Strategy for the Earth Observing System*, American Institute of Physics Press, Woodbury, N.Y., 1994.

Barath, F.T., et al., 'The Upper Atmosphere Research Satellite Microwave Limb Sounder Instrument,' *J. Geophys. Res. 98*, 10,751, 1993.

Borrman, S., S. Solomon, J.E. Dye, and B. Luo, 'The potential of cirrus clouds for heterogeneous chlorine activation,' *Geophys. Res. Lett. 23*, 1996.

Burrows, J.P., et al., 'The Global Ozone Monitoring Experiment (GOME): Mission Concept and First Scientific Results,' *J. Atmos. Sci. 56*, 151, 1999.

Cunnold, D., H.Wang, W.P. Chu, and L. Froidevaux, 'Comparisons between Stratospheric Aerosol and Gas Experiment II and microwave limb sounder ozone measurements and aliasing of SAGE II ozone trends in the lower stratosphere,' *J. Geophys. Res. 101*, 10,061, 1996a.

Cunnold, D., L. Froidevaux, J.M. Russell, B. Connor, and A. Roche, 'Overview of UARS ozone validation based primarily on intercomparisons among UARS and Stratospheric Aerosol and Gas Experiment II measurements,' *J. Geophys. Res. 101*, 10335, 1996b.

Elson, L.S., and L. Froidevaux, 'The use of Fourier transforms for asynoptic mapping: Early results from the Upper Atmosphere Research Satellite Microwave Limb Sounder, *J. Geophys. Res. 98*, 23039, 1993.

Filipiak, M.J., 'EOS MLS Retrieved Geophysical Parameter Precision Estimates', Edinburgh University Meteorology Department Technical Report (also Jet Propulsion Laboratory Document D-16160)**,** Version 1.1, 15 October 1999.

Fishbein, E.F., R.E. Cofield, L. Froidevaux, R.F. Jarnot, T.A. Lungu, W.G. Read, Z. Shippony, J.W. Waters, I.S. McDermid, T.J. McGee, U. Singh, M. Gross, A. Hauchecorne, P. Keckhut, M.E. Gelman, and R.M. Nagatani, 'Validation of UARS Microwave Limb Sounder temperature and pressure measurements,' *J. Geophys. Res. 101*, 9938, 1996.

Froidevaux, L., W.G. Read, T.A. Lungu, R.E. Cofield, E.F. Fishbein, D.A. Flower, R.F. Jarnot, B.P. Ridenoure, Z. Shippony, J.W. Waters, J.J. Margitan, I.S. McDermid, R.A. Stachnik, G.E. Peckham, G. Braathen, T. Deshler, J. Fishman, D.J. Hofmann, and S.J. Oltmans, 'Validation of UARS Microwave Limb Sounder ozone measurements,' *J. Geophys. Res. 101*, 10,017, 1996.

Froidevaux, L., et al., 'EOS MLS Science Data Validation Plan,' JPL D-18140, in preparation, 1999.

Hofmann, D.J., 'Recovery of antarctic ozone hole,' *Nature 384*, 222-223, 1996.

Jarnot, R.F., R.E. Cofield, J.W. Waters, G.E. Peckham, and D.A. Flower, 'Calibration of the Microwave Limb Sounder on the Upper Atmosphere Research Satellite,' *J. Geophys. Res. 101*, 9957, 1996.

Jarnot, R.F., 'EOS MLS Level 1 Data Processing Algorithm Theoretical Basis,' Jet Propulsion Laboratory Document D-15210**,** Version 1.1, 15 October 1999.

Jiang, Y.B., 'EOS MLS Level 3 Algorithms Theoretical Basis,' Jet Propulsion Laboratory Document D-NNNN, in preparation.

Lahoz, W.A., M.R. Suttie, L. Froidevaux, R.S. Harwood, C.L. Lau, T.A. Lungu, G.E. Peckham, H.C. Pumphrey, W.G. Read, Z. Shippony, R.A. Suttie, J.W. Waters, G.E. Nedoluha, S.J. Oltmans, J. Russell III, and W.A. Traub, 'Validation of UARS Microwave Limb Sounder 183 GHz $H_2O$ measurements,' *J. Geophys. Res. 101*, 10,129, 1996.

Lindzen, R.S., 'Some coolness concerning global warming,' *Bull. Am. Meteorol. Soc. 71*, 288-299, 1990.

Livesey, N.J., and D.L. Wu, 'EOS MLS Retrieval Processes Algorithm Theoretical Basis,' Jet Propulsion Laboratory Document D-16159**,** Version 1.1, 15 October 1999.

Livesey, N.J., and W.G. Read, 'Direct Retrieval of Line-of-Sight Atmospheric Structure from Limb Sounding Observations, *Geophys. Res. Lett.*, submitted 1999.

Mackenzie, I., R.S. Harwood, L. Froidevaux, W.G. Read, and J.W. Waters, 'Chemical loss of polar vortex ozone inferred from UARS MLS measurements of ClO during the Arctic and Antarctic springs of 1993', *J. Geophys. Res. 101*, 14505-14518, 1996.

Manney, G.L., L. Froidevaux, J.W. Waters, R.W. Zurek, W.G. Read, L.S. Elson, J.B. Kumer, J.L. Mergenthaler, A.E. Roche, G.E. Peckham, and R. Swinbank, 'Chemical depletion of ozone in the Arctic lower stratosphere during winter 1992-93, *Nature 370*, 429-434, 1994.

McPeters, R.D., S.M. Hollandsworth, L.E. Flynn, J.R. Herman, and C.J. Seftor, 'Long-term ozone trends derived from the 16-year combined Nimbus 7/Meteor 3 TOMS Version 7 record,' *Geophys. Res. Lett. 23*, 3699, 1996.

MTPE EOS Reference Handbook 1995, available from the EOS Project Science Office, code 900, NASA Goddard Space Flight Center, Greenbelt, MD 20771, 1995.

NASA Goddard Space Flight Center, 'EOS Execution Phase Project Plan,' GSFC document 170-01-01, May 1995.

NASA Goddard Space Flight Center, EOS Chemistry Project Plan, GSFC Document 424-PG-7120.2.1, 15 April 1999.

NASA Reference Publication 1399, 'Present State of Knowledge of the Upper Atmosphere 1996: An Assessment Report,' 1997.

Oh, J.J., and E.A. Cohen, 'Pressure broadening of ClO by $N_2$ and $O_2$ near 204 and 649 GHz and new frequency measurements between 632 and 725 GHz,' *J. Quant. Spectrosc. Radiat. Transfer 54*, 151-156, 1994.

Pickering, K.E., A.M. Thompson, Y. Wang, W. Tao, D.P. McNamara, V. W. J. H. Kirchhoff, B.G. Heikes, G.W. Sachse, J.D. Bradshaw, G.L. Gregory, and D.R. Blake, 'Convective transport of biomass burning emissions over Brazil during TRACE A,' *J. Geophys. Res. 101*, 23,993, 1996.

Pickett, H.M., R.L. Poynter, and E.A. Cohen, 'Submillimeter, Millimeter, and Microwave Spectral Line Catalog, *Tech. Rep. 80-23*, Jet Propulsion Laboratory, Pasadena, California, 1992.

Pickett, H.M., 'THz spectroscopy of the atmosphere,' *SPIE 3617*, 2-6, 1999.

Pierrehumbert, R.T., 'Thermostats, radiator fins, and local runaway greenhouse,' *J. Atmos. Sci. 52*, 1754-1806, 1995.

Read, W.G., L. Froidevaux, and J.W. Waters, 'Microwave Limb Sounder (MLS) measurements of $SO_2$ from Mt. Pinatubo volcano,' *Geophys. Res. Lett. 20*, 1299, 1993.

Read, W.G., J.W. Waters, L. Froidevaux, D.A. Flower, R.F. Jarnot, D.L. Hartmann, R.S. Harwood, and R.B. Rood, 'Upper-tropospheric water vapor from UARS MLS,' *Bull. Am. Meteorol. Soc. 76*, 2381, 1995.

Read, W.G., et al., 'EOS MLS Forward Model Theoretical Basis', Jet Propulsion Laboratory Document D-NNNN (in preparation)**,** 1999.

Reber, C.A., C.E. Trevathan, R.J. McNeal, and M.R. Luther, 'The Upper Atmosphere Research Satellite (UARS) mission', *J. Geophys. Res. 98*, 10,643, 1993.

Reichardt, J., A. Ansmann, M. Serwazi, C. Weitkamp, and W. Michaelis, 'Unexpectedly low ozone concentration in midlatitude tropospheric ice clouds: a case study,' *Geophys. Res. Lett. 23*, 1929, 1996.

Ricaud, P., J. de La Noe, B.J. Connor, L.Froidevaux, J.W. Waters, R.S. Harwood, I.A. MacKenzie, and G.E. Peckham, 'Diurnal variability of mesospheric ozone as measured by the UARS microwave limb sounder instrument: Theoretical and ground-based validations,' *J. Geophys. Res. 101*, 10,077, 1996.

Rodgers, C.D., 'Retrieval of atmospheric temperature and composition from remote measurements of thermal radiation, *Reviews of Geophysics and Space Physics 14*, 609, 1976.

Rodgers, C.D., 'Characterization and error analysis of profiles retrieved from remote sounding measurements,' *J. Geophys. Res. 95*, 5587, 1990.

Salby, M.L., 'Sampling theory for asynoptic satellite observations. Part I: Space-time spectra, resolution and aliasing,' *J. Atmos. Sci. 39*, 2577, 1982.

Sandor, B.J., W.G. Read, J.W. Waters, K.H. Rosenlof, 'Seasonal behavior of tropical to midlatitude upper tropospheric water vapor from UARS MLS,' *J. Geophys. Res. 103*, 25935-25947, 1998.

Santee, M.L., W.G. Read, J.W. Waters, L. Froidevaux, G.L. Manney, D.A. Flower, R.F. Jarnot, R.S. Harwood, and G.E. Peckham, 'Interhemispheric differences in polar stratospheric $HNO_3$, $H_2O$, ClO and $O_3$,' *Science 267*, 849, 1995.

Schoeberl, M.R., R.S. Stolarski, A.R. Douglass, P.A. Newman, L.R. Lait, and J.W. Waters, 'MLS ClO observations and arctic polar vortex temperatures,' *Geophys. Res. Lett. 20*, 2861-2854, 1993.

Shindell, D.T., D. Rind, P. Lonergan, 'Increased polar stratospheric ozone losses and delayed eventual recovery owing to increasing greenhouse gas concentrations,' *Nature 392*, 589-592, 1998.

Siegel, P.H., I. Mehdi, R.J. Dengler, J.E. Oswald, A. Pease, T.W. Crowe, W. Bishop, Y. Li, R.J. Mattauch, S. Weinreb, J. East, and T. Lee, 'Heterodyne radiometer development for the Earth Observing System Microwave Limb Sounder,' in *Infrared and Millimeter-Wave Engineering, SPIE 1874*, 124, 1993.

Solomon, S., S. Borrmann, R.R. Garcia, R. Portmann, L. Thomason, L.R. Poole, D. Winker, and M.P. McCormick, 'Heterogeneous chlorine chemistry in the tropopause region,' *J. Geophys. Res. 102*, 21411, 1997.

Solomon, S., 'Stratospheric Ozone Depletion: A Review of Concepts and History,' *Rev. Geophys. 37*, 275, 1999.

Stachnik, R.A., J.C. Hardy, J.A. Tarsala, J.W. Waters, and N.R. Erickson, 'Submillimeterwave heterodyne measurements of stratospheric ClO, HCl, $O_3$, and $HO_2$: First results,' *Geophys. Res. Lett. 19*, 1931, 1992.

Subcommittee on Global Change Research, 'Our Changing Planet: The FY99 U.S. Global Change Research Program,' a supplement to the President's Fiscal Year 1999 budget, available from the Global Change Research Information Office User Services, 2250 Pierce Road, University Center MI 48710 (http://www.gcrio.org). Document available on-line at http://www.gcrio.org/ocp99/toc.html, 1998.

Thompson, A.M., 'The Oxidizing Capacity of Earth's Atmosphere: Probable Past and Future Changes,' *Science 256*, 1157-1165, 1992.

Thompson, A.M., K.E. Pickering, D.P. McNamara, M.R. Schoeberl, R.D. Hudson, J.H. Kim, E.V. Browell, V. W. J. H. Kirchhoff, and D. Nganga, 'Where did tropospheric ozone over southern Africa and the tropical Atlantic come from in October 1992? Insights from TOMS, GTE TRACE A, and SAFARI 1992', *J. Geophys. Res. 101*, 24278, 1996.

Thompson, D.W.J., and J.M. Wallace, 'The Arctic Oscillation signature in the wintertime geopotential height and temperature fields,' *Geophys. Res. Lett. 25*, 1297, 1998.

Wang, Y., and D.J. Jacob, 'Anthropogenic forcing on tropospheric ozone and OH since preindustrial times,' *J. Geophys. Res. 103*, 31123-31135, 1998.

Waters, J.W. J.J. Gustincic, R.K. Kakar, H.K. Roscoe, P.N. Swanson, T.G. Phillips, T. DeGraauw, A.R. Kerr, and R.J. Mattauch, 'Aircraft search for millimeter wavelength emission by stratospheric ClO,' *J. Geophys. Res. 84,* 6934, 1979.

Waters, J.W., J.C. Hardy, R.F. Jarnot, and H.M. Pickett, 'Chlorine monoxide radical, ozone, and hydrogen peroxide: Stratospheric measurements by microwave limb sounding,' *Science 214*, 61, 1981.

Waters, J.W., 'Microwave Limb Sounding,' in *Atmospheric Remote Sensing by Microwave Radiometry* (M.A. Janssen, ed.), chapter 8, New York: John Wiley, 1993.

Waters, J.W., W.G. Read, L. Froidevaux, T.A. Lungu, V.S. Perun, R.A. Stachnik, R.F. Jarnot, R.E. Cofield, E.F. Fishbein, D.A. Flower, J.R. Burke, J.C. Hardy, L.L. Nakamura, B.P. Ridenoure, Z. Shippony, R.P. Thurstans, L.M. Avallone, D.W. Toohey, R.L. deZafra, and D.T. Shindell, 'Validation of UARS Microwave Limb Sounder ClO measurements,' *J. Geophys. Res. 101*, 10,091, 1996.

Waters, J.W., W.G. Read, L. Froidevaux, R.F. Jarnot, R.E. Cofield, D.A. Flower, G.K. Lau, H.M. Pickett, M.L. Santee, D.L. Wu, M.A. Boyles, J.R. Burke, R.R. Lay, M.S. Loo, N.J. Livesey, T.A. Lungu, G.L. Manney, L.L. Nakamura, V.S. Perun, B.P. Ridenoure, Z. Shippony, P.H. Siegel, R.P. Thurstans, R.S. Harwood, H.C. Pumphrey, M.J. Filipiak, 'The UARS and EOS Microwave Limb Sounder Experiments,' *J. Atmos. Sci. 56*, 194-218, 1999.

Weinreb, S., P.C. Chao, and W. Copp, 'Full Waveguide Band, 90 to 140 GHz MMIC Amplifier Module,' *1997 IEEE MTT-S Digest*, 127, 1997.

Wu, D.L., and J.W. Waters, 'Gravity-wave-scale temperature fluctuations seen by the UARS MLS,' *Geophys. Res. Lett. 23*, 3289, 1996.